

Published in final edited form as:

Sci Signal. ; 13(618): . doi:10.1126/scisignal.aaw6923.

L-type Ca²⁺ channel-mediated Ca²⁺-influx adjusts neuronal mitochondrial function to physiological and pathophysiological conditions

Matej Hotka^{1,*}, Michal Cagalinec^{1,2,3}, Karlheinz Hilber¹, Livia Hool^{4,5}, Stefan Boehm¹, Helmut Kubista^{1,*}

¹Center of Physiology and Pharmacology, Department of Neurophysiology and Neuropharmacology, Medical University of Vienna, Waehringerstrasse 13a, 1090, Vienna, Austria

²Dept. of Cellular Cardiology, Institute of Experimental Endocrinology, Biomedical Research Center, Slovak Academy of Sciences, Dubravska cesta 9, 845 05 Bratislava, Slovakia

³Laboratory of Mitochondrial Dynamics, Department of Pharmacology, Institute of Biomedicine and Translational Medicine, Faculty of Medicine, University of Tartu, Ravila 19, 50 411 Tartu, Estonia

⁴School of Human Sciences (Physiology), The University of Western Australia, Crawley, WA, 6009, Australia

⁵Victor Chang Cardiac Research Institute, Sydney, NSW, 2010, Australia

Abstract

L-type voltage-gated Ca²⁺ channels (LTCCs) are implicated in neurodegenerative processes and cell death. Accordingly, LTCC antagonists have been proposed to be neuroprotective although this view is disputed, because intentional LTCC activation can also have beneficial effects. LTCC-mediated Ca²⁺ influx influences mitochondrial function, which plays a crucial role in the regulation of cell viability. Hence, we investigated the effect of modulating LTCC-mediated Ca²⁺ influx on mitochondrial function in cultured hippocampal neurons. To activate LTCCs, neuronal activity was stimulated by increasing extracellular K⁺ or by application of the GABA_A receptor antagonist bicuculline. The activity of LTCCs was altered by application of an agonistic (Bay K8644) or an antagonistic (isradipine) dihydropyridine. Our results demonstrated that activation of LTCC-mediated Ca²⁺ influx affected mitochondrial function in a bimodal manner. At moderate stimulation strength, ATP synthase activity was enhanced, an effect that involved Ca²⁺-induced Ca²⁺-release from intracellular stores. In contrast, high LTCC-mediated Ca²⁺ loads led to a switch

*To whom correspondence should be addressed: Matej Hotka (matej.hotka@meduniwien.ac.at) and Helmut Kubista (helmut.kubista@meduniwien.ac.at).

Author contributions: M.H. and H.K. conceived the original idea in consultation with M.C. M.H. and H.K. performed the experiments and analyzed the data. K.H. and S.B. aided in interpreting the results and in drafting the manuscript. H.K. and M.H. wrote the manuscript. S.B., L. H. and M. C. revised the manuscript. All authors discussed the results and contributed to the final manuscript.

Competing interests: The authors declare that they have no competing interests.

“This manuscript has been accepted for publication in Science Signaling. This version has not undergone final editing. Please refer to the complete version of record at <http://www.sciencesignaling.org/>. The manuscript may not be reproduced or used in any manner that does not fall within the fair use provisions of the Copyright Act without the prior, written permission of AAAS.”

in ATP synthase activity to reverse mode operation. This effect, which required nitric oxide, helped to prevent mitochondrial depolarization and sustained increases in mitochondrial Ca^{2+} . Our findings indicate a complex role of LTCC-mediated Ca^{2+} influx in the tuning and maintenance of mitochondrial function. Therefore, the use of LTCC inhibitors to protect neurons from neurodegeneration should be reconsidered carefully.

Editor's summary: A reversal to limit neuronal death

Ca^{2+} ions are an important second messenger, but excessive Ca^{2+} mitochondrial influx from the cytoplasm can trigger cell death. In response to depolarizing stimuli, L-type Ca^{2+} channels mediate Ca^{2+} entry into neurons. Hotka *et al.* found that the effect of L-type Ca^{2+} channel activity on mitochondrial Ca^{2+} concentrations depended on the strength of the depolarizing stimulus applied to neurons. Stimuli of moderate strength enhanced the production of ATP by ATP synthase. In contrast, stronger depolarizing stimuli caused the ATP synthase to operate in reverse mode and consume ATP, which helped to limit increases in mitochondrial Ca^{2+} . These results may explain why neuroprotection is seen not only with blockers of L-type Ca^{2+} channel activity, but also with compounds that stimulate channel activity.

Introduction

L-type voltage-gated Ca^{2+} channels (LTCCs) are involved in many different neurophysiological functions, including synaptic plasticity, neuronal excitability and Ca^{2+} -dependent gene transcription (reviewed by Berger and Bartsch (1)). However, there is increasing evidence of enhanced LTCC activity in neurodegenerative diseases, such as Alzheimer's disease and Parkinson's disease (2), and increased abundance or activity of LTCCs has been associated with neuronal damage (3–5). Moreover, LTCCs appear to provide a route of Ca^{2+} entry in ischemic injury-induced excitotoxicity (6). Hence, the blockade of LTCCs has been suggested as therapeutic principle to achieve neuroprotection (7). Unfortunately, the use of LTCC antagonists in studies on animal models of neurodegenerative diseases has yielded controversial results (8), and clinical trials, such as in stroke patients, failed to demonstrate efficacy of LTCC inhibitors (9–11). Furthermore, beneficial effects of LTCCs in neuronal injury have also been observed, leading to the proposal that LTCC activation rather than inhibition is neuroprotective (12, 13).

Effects of enhanced LTCC activity on neurons have been repeatedly linked to altered mitochondrial function (14–17). Detrimental effects are most commonly attributed to mitochondrial Ca^{2+} overload (14, 15, 17). On the other hand, Ca^{2+} influx during neuronal activity stimulates mitochondrial metabolism (18, 19), but little is known about the exact Ca^{2+} entry pathway involved in this regulation (20). LTCCs are one candidate for providing Ca^{2+} rises that might regulate mitochondria. Hence, the aim of this study was to explore effects of different levels of LTCC-mediated Ca^{2+} influx on mitochondrial function. Elevated concentrations of extracellular K^+ have been widely used to elicit LTCC-mediated Ca^{2+} influx to study the role of LTCCs in neuronal development and viability (21–24). Using this approach, we assayed mitochondrial function with the ATP synthase inhibitor

oligomycin while monitoring the ATP/ADP ratio and mitochondrial membrane potential with fluorescence indicators. Additionally, LTCCs were activated by induction of neuronal firing using the gamma-aminobutyric acid type A (GABA_A) receptor antagonist bicuculline. Our results suggest a bimodal regulation of the mitochondrial ATP synthase by LTCC-mediated Ca²⁺ influx. ATP generation was stimulated at moderate Ca²⁺ elevations, but reverse mode operation (RMO) was induced at more pronounced levels of LTCC-mediated Ca²⁺ influx, whereby ATP synthase consumes ATP. We provide evidence that RMO played a role in maintaining the mitochondrial membrane potential. In parallel to the induction of RMO, the accompanying mitochondrial Ca²⁺ elevations became transient. Formation of nitric oxide played a role in both potentially neuroprotective mechanisms. Together, these effects on mitochondrial function may provide a basis for the understanding of the controversial role of LTCCs in neuroprotection and/or neurodegeneration.

Results

K⁺-stimulation of hippocampal neurons alters the effect of ATP synthase inhibition on the cytosolic ATP/ADP ratio

We first addressed the effects of LTCC-mediated Ca²⁺ influx on mitochondrial function by monitoring the cytosolic ATP/ADP ratio using the fluorescence indicator Perceval (fig. S1A). We probed the contribution of ATP produced by the mitochondrial ATP synthase by using the specific inhibitor oligomycin. The use of oligomycin also provided information regarding the operational mode of the mitochondrial ATP synthase. LTCC-mediated Ca²⁺ influx was triggered by stimulation of neuronal activity with high-K⁺ solutions and was increased and decreased by application of the dihydropyridine-type LTCC modulators Bay K8644 (BayK, agonist) and isradipine (Isra, antagonist), respectively.

Raising external K⁺ from the standard concentration of 4 mM to 10 mM, which depolarized hippocampal neurons and enhanced neuronal electrical activity (fig. S2A), led to a drop in the ATP/ADP ratio (Fig. 1A, black trace). For readability, the y-axes in the figures are always labeled according to the represented variable rather than to the normalized fluorescence of the fluorescent indicator (for example, ATP/ADP instead of Perceval403/488 fluorescence in Fig. 1A). Addition of oligomycin caused a pronounced further drop, which was indicative of a prominent contribution of the mitochondrial ATP synthase to ATP production (Fig. 1A, black trace). When external K⁺ was increased to 20 mM, which caused depolarized plateau potentials in hippocampal neurons (fig. S2A), the drop in ATP/ADP ratio was augmented, but treatment with oligomycin under this condition led to a signal reversal (causing a relative increase in Perceval fluorescence). This finding demonstrated that an oligomycin-sensitive mechanism was actually contributing to the initial decrease in the ATP/ADP ratio (Fig. 1A, blue trace). A similar response was observed when 10 mM K⁺ was applied together with BayK (Fig. 1A, green trace), which also caused depolarized plateau potentials (fig. S2B). The signal reversal after oligomycin application indicated a shift to RMO of mitochondrial ATP synthase, in which mitochondria turned into consumers of ATP (25), and thus blocking ATP synthase in the reverse mode attenuated the drop in the ATP/ADP ratio. Moreover, we demonstrated that the large drops in ATP/ADP ratio recovered after the stimulations, which suggests that neurons were not metabolically harmed

(fig. S3, A and B). Many fluorescent probes show pH-dependent sensing, a feature that also applies to Perceval (26). However, our stimulation paradigms did not substantially change intracellular pH, as revealed by the pH indicator pHRED and NH_4Cl as a positive control (fig. S4, A and B). Hence, no corrections for potential pH bias were required.

In the presence of 4 mM K^+ , the application of oligomycin only slightly decreased the ATP/ADP ratio, suggesting that in an unstimulated, resting state of neuronal activity little ATP was generated by the mitochondrial ATP synthase (Fig. 1A, purple trace). It could be inferred from the direction and the magnitude of the oligomycin effect that although stimulation with 10 mM K^+ led to an augmentation of ATP synthase activity, stimulation with 20 mM K^+ and with 10 mM K^+ + BayK induced RMO, as evidenced by a relative increase in the ATP/ADP ratio.

K^+ -dependent regulation of the ATP synthase requires cytosolic Ca^{2+} elevations

Next, we sought to confirm that the observed changes in ATP synthase activity upon K^+ stimulation were caused by intracellular Ca^{2+} elevations. To address this question, we pre-loaded neurons with the Ca^{2+} -chelator BAPTA-AM. Stimulation with 10 mM K^+ in BAPTA-loaded neurons did not cause an obvious drop in the ATP/ADP ratio (Fig. 1B, black trace) and did not augment the effect of oligomycin in comparison to the small drop in ATP/ADP ratio caused by oligomycin in the presence of 4 mM K^+ (Fig. 1B, purple trace). Stimulation with 20 mM K^+ evoked a pronounced drop in the ATP/ADP ratio, but subsequent addition of oligomycin did not cause a reversal of the signal but instead caused a further decrease (Fig. 1B, blue trace). Similarly, when 10 mM K^+ was applied together with BayK to potentiate LTCC-mediated Ca^{2+} influx (Fig. 1B, green trace) the drop in the ATP/ADP ratio was more pronounced than with 10 or 20 mM K^+ , yet oligomycin application still did not reveal any signs of ATP synthase operating in the reverse mode. Statistical analysis revealed that the oligomycin-dependent changes under activating conditions (10 mM, and 20 mM K^+ ; 10 mM K^+ + BayK) were significantly different from those under resting conditions (4 mM K^+), but only in neurons that had not been exposed to BAPTA-AM (Fig. 1C). These data indicated that the augmentation of ATP synthase activity as well as the switch to RMO required increases in free cytosolic Ca^{2+} concentrations.

The Ca^{2+} -mediated regulation of the ATP synthase shows source specificity

To specifically address the implication of LTCC-mediated Ca^{2+} -influx in this phenomenon, we repeated the previous experiments in the presence of the LTCC inhibitor isradipine. When neurons were stimulated with 10 (Fig. 1D, red trace) or 20 mM K^+ (Fig. 1D, orange trace), the drop in the ATP/ADP ratio was considerably smaller in the presence than in the absence of isradipine (compare traces in Fig. 1D with those in Fig. 1A). Moreover, subsequent addition of oligomycin failed to elicit any additional change in the ATP/ADP ratio (Fig. 1D). Similar observations were made when LTCCs were inhibited with the non-dihydropyridine type LTCC blocker diltiazem (fig. S5), arguing against an off-target effect of the dihydropyridine on ATP synthase or related proteins. When neurons were treated with an even higher external K^+ concentration (30 mM) in the presence of isradipine, the drop in ATP/ADP exceeded those observed with stimulations with lower K^+ concentrations (including those seen in the absence of isradipine, Fig. 1A) and it was not affected by

oligomycin (Fig. 1D, purple trace). These findings indicated that LTCC-dependent Ca^{2+} -influx was required for both the stimulation of the ATP synthase (as evidenced by a pronounced decrease in the ATP/ADP ratio upon application of oligomycin) and the switch to RMO of the ATP synthase (as evidenced by the relative increase in the ATP/ADP ratio upon application of oligomycin).

To further substantiate that cytosolic Ca^{2+} elevations independent of LTCC gating did not affect the ATP synthase, applications of glutamate (10, 30 and 100 μM) were followed by the addition of oligomycin. These experiments were performed in the presence of isradipine (Fig. 1E) to prevent gating of LTCCs due to glutamate-induced depolarization (exemplar traces of glutamate-induced voltage responses are shown in fig. S2C). Although a distinct drop in the ATP/ADP ratio was evoked by all three concentrations of glutamate, particularly by 30 μM and 100 μM glutamate, oligomycin had no additional effect. Hence, oligomycin led neither to signs of ATP synthase stimulation (for example at 10 μM glutamate) nor of RMO (at 30 and 100 μM glutamate), which further supports the conclusion that Ca^{2+} -dependent ATP synthase reversal was source-specific.

To further corroborate this claim, we used the fluorescent cytosolic Ca^{2+} ($[\text{Ca}^{2+}]_{\text{cyt}}$) indicator Fluo-4 (fig. S1B) to compare Ca^{2+} rises evoked by K^+ elevations and glutamate. Isradipine was used to test for the role of LTCCs in high- K^+ solutions (Fig. 1, F to G) or to prevent their contribution in the presence of glutamate (Fig. 1H). Application of 10 and 20 mM K^+ for 5 minutes evoked cytosolic Ca^{2+} transients which were followed by a plateau phase of Ca^{2+} elevation that lasted for the entire duration of the high- K^+ stimulation (Fig. 1, F to G). Isradipine application (Fig. 1F, red trace) revealed a small but distinct contribution of LTCCs in 10 mM K^+ (Fig. 1F, black trace) which was considerably increased upon potentiation of LTCCs with BayK (Fig. 1F, green trace). A large contribution of LTCCs was also seen with 20 mM K^+ , particularly during the plateau phase of the evoked Ca^{2+} elevations (Fig. 1G). In contrast to K^+ -stimulation, glutamate (30 and 100 μM in the presence of isradipine) evoked pronounced elevations of $[\text{Ca}^{2+}]_{\text{cyt}}$ that showed much less decline within 5 minutes of application (Fig. 1H). Hence, these results collectively (Fig. 1, A to H) suggest that Ca^{2+} rises provided by LTCCs specifically modulate the function of mitochondrial ATP synthase.

Effects of oligomycin on the mitochondrial membrane potential confirm the bimodal regulation of the ATP synthase by LTCC-mediated Ca^{2+} influx

To test the effect of LTCC-mediated Ca^{2+} influx on the operational mode of the mitochondrial ATP synthase using an alternative methodological approach, we also probed the effect of oligomycin on the mitochondrial membrane potential (Ψ_{mt}) using the Ψ_{mt} -indicator dye tetramethylrhodamine methyl ester (TMRM) (fig. S1C), an experiment that has been named the oligomycin null-point test (27). Oligomycin causes hyperpolarization of Ψ_{mt} by blocking proton re-entry when ATP synthase is operating in forward mode and depolarization due to reduction of proton extrusion when it acts in reverse mode (28). Glutamate (30 μM) evoked a large drop in TMRM fluorescence, indicating pronounced mitochondrial depolarization (Fig. 2A, purple trace). Addition of oligomycin did not cause any obvious fluorescence change. In the presence of isradipine, stimulation with 10 mM K^+

or application of oligomycin did not substantially affect TMRM fluorescence (Fig. 2A, red trace), indicating a low rate of ATP production in this case. In contrast, with operating LTCCs (that is, in the absence of isradipine), 10 mM K⁺ evoked a hyperpolarization of the mitochondrial membrane potential (reflected by a fluorescence increase), which was further augmented by oligomycin (Fig. 2A, black trace). This hyperpolarization is indicative of increased respiration and the effect of oligomycin reflects an inhibition of proton influx through ATP synthase in mitochondria synthesizing ATP. Application of 10 mM K⁺ + BayK evoked an even larger hyperpolarization of the mitochondrial membrane potential, but oligomycin then led to a decrease in the TMRM fluorescence indicative of mitochondrial depolarization (Fig. 2A, green trace). At the end of all these experiments, the mitochondrial uncoupler FCCP led to a depolarization as revealed by the decrease in fluorescence (Fig. 2A).

Quantification and statistical evaluation of TMRM data showed that oligomycin did not cause a significant change in Ψ_{mt} when neurons were challenged by either 10 mM K⁺ + isradipine or by 30 μM glutamate (P values = 0.16; paired t-test). However, the values of Ψ_{mt} obtained in all the other conditions were significantly different from those calculated for 10 mM K⁺ + isradipine or 30 μM glutamate (Fig. 2B). These results demonstrate a hyperpolarization (+ Ψ_{mt}) by oligomycin in 10 mM K⁺ and a depolarization (- Ψ_{mt}) in 10 mM K⁺ + BayK, respectively. Furthermore, they parallel the results of ATP/ADP measurements, which led us to conclude that moderate stimulation of LTCC activity with 10 mM K⁺ stimulates mitochondrial ATP production, whereas pronounced stimulation of LTCC activity (with 10 mM K⁺ + BayK) turns mitochondria into consumers of ATP. The hyperpolarization of Ψ_{mt} elicited by moderate stimulation of LTCCs can be explained by an increased extrusion of protons into the intermembrane space in the course of enhanced respiratory activity of the mitochondrial electron transport chain. Mitochondrial hyperpolarization during pronounced stimulation of LTCCs may be supported by ATP synthase running in reverse mode, which would likewise depend on proton extrusion. To test this possibility, we first inhibited ATP synthase by oligomycin and then monitored the effect of 10 mM K⁺ + BayK on Ψ_{mt} . In the absence of oligomycin pretreatment, Ψ_{mt} was hyperpolarized (Fig. 2C, green trace). In contrast, oligomycin pre-applied before 10 mM K⁺ + BayK resulted in Ψ_{mt} depolarization (Fig. 2C, gray trace). Thus, the observed hyperpolarization was directly mediated by ATP synthase.

LTCC-mediated Ca²⁺ influx regulates mitochondrial ATP synthase during bicuculline-induced neuronal firing

To confirm the results obtained with sustained K⁺-induced depolarizations (fig. S2, A and B), more physiological neuronal firing was induced by the GABA_A receptor inhibitor bicuculline (1 μM) and the LTCC availability was modulated again with dihydropyridines (fig. S6A). Neuronal firing during normal LTCC availability (in the absence of BayK or isradipine) led to mitochondrial hyperpolarization as evidenced by an increase in TMRM fluorescence (Fig. 2D, black trace). Oligomycin application resulted in an additional increase in TMRM fluorescence, indicating that mitochondria were operating in the ATP producing mode. When bicuculline (1 μM) was co-applied with BayK, mitochondria transiently hyperpolarized (Fig. 2D, green trace), but the initial increase in TMRM

fluorescence was followed by a decrease slightly below baseline, and oligomycin further reduced TMRM fluorescence. These findings suggest that Ψ_{mt} settled at a moderately depolarized level in these cells, presumably sustained by RMO of the ATP synthase. Indeed, in contrast to glutamate, which caused a collapse of Ψ_{mt} and which did not induce obvious signs of RMO (Fig. 2A, purple trace), stimulation with 1 μ M bicuculline + BayK did not lead to severe depolarization of Ψ_{mt} , although this treatment triggered pronounced discharge activity (fig. S6A). Effects on Ψ_{mt} were largely reduced but not abolished when isradipine was co-applied with bicuculline (Fig. 2D, red trace). Likewise, the presence of isradipine reduced but did not abolish bicuculline (1 μ M)-induced neuronal firing (fig. S6A).

To further increase the intensity of neuronal discharge, we raised the concentration of bicuculline to 10 μ M (fig. S6B). Firing induced by 10 μ M Bic did not affect Ψ_{mt} (Fig. 2E, black trace), and the time course of TMRM fluorescence was similar to that obtained with co-application of bicuculline (10 μ M) and isradipine (Fig. 2E, red trace). However, oligomycin caused hyperpolarization (as shown by the increase in TMRM fluorescence) in the absence of isradipine, but not in the presence of isradipine. In contrast, when LTCCs were potentiated with BayK (Fig. 2E, green trace), bicuculline-induced firing resulted in a moderate decrease in TMRM fluorescence, indicative of partial mitochondrial depolarization, but not in a collapse of Ψ_{mt} as seen with glutamate (Fig. 2A, purple trace) or with nominally Mg^{2+} -free external solution (Fig. 2E, purple trace), which we included to evoke pronounced “seizure-like activity” by removing the Mg^{2+} -block of NMDA (N-methyl-D-aspartate)-type glutamate receptors ((29) and fig. S6C). Oligomycin application again revealed that only the moderate decrease in TMRM fluorescence by bicuculline (10 μ M) + BayK was accompanied (and probably restrained) by RMO of ATP synthase. To corroborate this claim, we monitored the TMRM fluorescence change induced by bicuculline (1 μ M) + BayK when ATP synthase had been blocked by oligomycin. In the absence of oligomycin and therefore unimpaired ATP synthase, neuronal firing induced by bicuculline (1 μ M) + BayK caused transient hyperpolarization of Ψ_{mt} , which was followed by a return to a level slightly more depolarized than the baseline before stimulation (Fig. 2F, green trace). Subsequent application of oligomycin caused further depolarization, which revealed that Ψ_{mt} was maintained by ATP synthase operating in reverse mode. When oligomycin was pre-applied, thereby preventing reversal of the ATP synthase (Fig. 2F, gray trace), neuronal firing induced by bicuculline (1 μ M) + BayK resulted in depolarization of Ψ_{mt} , which started immediately after the stimulation had been initiated. This result showed that the RMO of ATP synthase mediated a hyperpolarizing force on Ψ_{mt} during neuronal firing induced by bicuculline + BayK.

Different mitochondrial matrix Ca^{2+} signals accompany the bimodal LTCC-dependent regulation of mitochondrial function

One mechanism that may link LTCC-mediated Ca^{2+} influx through the plasma membrane to ATP synthase activity is a corresponding rise of Ca^{2+} in the mitochondrial matrix. To explore this possibility, we used CEPIA2mt (fig. S1G) to monitor mitochondrial Ca^{2+} rises ($[Ca^{2+}]_{mt}$). 10 mM K^+ caused slow and small increases in $[Ca^{2+}]_{mt}$ (Fig. 3A, black trace). Mitochondrial Ca^{2+} rises were faster and larger but transient when neurons were stimulated with either 10 mM K^+ + BayK (Fig. 3A, green trace) or 20 mM K^+ (Fig. 3B, blue trace).

These transient Ca^{2+} signals were LTCC-mediated, because they were blocked by isradipine (Fig. 3B, orange trace). Notably, they were followed by an apparent release of mitochondrial Ca^{2+} in the later phases of the responses as evidenced by a drop in the fluorescence signal below baseline starting at about 350 seconds after the start of recording (Fig. 3, A and B). In contrast, 10, 30 and 100 μM glutamate evoked strong rises in $[\text{Ca}^{2+}]_{\text{mt}}$ that showed a sustained plateau, in particular with 30 and 100 μM glutamate (Fig. 3C). This mitochondrial Ca^{2+} response pattern allowed for repeated elicitation of Ca^{2+} signals in response to stimulation with high K^+ and BayK (Fig. 3D), demonstrating that mitochondria could still resolve individual stimuli. In contrast, glutamate caused persistent Ca^{2+} elevations in mitochondria (Fig. 3E). Together, ATP synthase reversal (Fig. 1A, green trace and blue trace) occurred during sustained LTCC-mediated cytosolic Ca^{2+} responses (Fig. 1F, green trace; Fig. 1G, blue trace) and was associated with a transient pattern of mitochondrial Ca^{2+} elevation (Fig. 3A, green trace; Fig. 3B, blue trace). In contrast, sustained cytosolic Ca^{2+} responses induced by glutamate (Fig. 1H), which gave rise to long-lasting Ca^{2+} elevations in the mitochondrial matrix (Fig. 3C), did not lead to ATP synthase reversal. These data indicated that source rather than magnitude of Ca^{2+} elevations determined the operational switch of ATP synthase.

The sustained LTCC-mediated cytosolic Ca^{2+} rises do not induce neuronal death

Cytosolic and mitochondrial Ca^{2+} overload has been linked to cell death (30). We therefore examined the effect of our stimulations on cell viability with propidium iodide (PI) uptake assays (fig. S1D). After 30 hours of incubation, neither 20 mM K^+ nor 10 mM K^+ + BayK promoted neuronal death. Hence, reverse mode operation of ATP synthase was not accompanied by an increase in neuronal death. On the other hand, treatment of the neurons with 100 μM glutamate led to a pronounced increase in PI-positive neurons, indicative of widespread neuronal death (Fig. 3F).

In addition, we also looked at changes of mitochondrial morphology, which are thought to be linked to bioenergetic functionality (31). Exposure of neurons labeled with mito-DsRed to 30 μM (or 100 μM) glutamate for 5 minutes caused mitochondrial fragmentation which was irreversible within the time frame of our experiments (about 45 minutes) (Fig. 3G). Although stimulation with 10 mM K^+ + BayK also led to widespread mitochondrial fragmentation, this effect was fully reversible within 15 minutes after replacement with control solution containing 4 mM K^+ (Fig. 3H and Movie S1).

The bimodal regulation of mitochondrial function by LTCC-mediated Ca^{2+} influx occurs by means of different signaling pathways

LTCC-dependent cytosolic Ca^{2+} rises are augmented by Ca^{2+} -induced Ca^{2+} release (CICR) from the endoplasmic reticulum (32). To test for a role of CICR in the LTCC-dependent regulation of mitochondrial function, we depleted Ca^{2+} stored in the endoplasmic reticulum by pre-treating neurons with the SERCA (sarco/endoplasmic reticulum Ca^{2+} -ATPase)-inhibitor thapsigargin. In neurons with depleted ER, 10 mM K^+ initially decreased the ATP/ADP ratio (Fig. 4A, orange trace) in a fashion similar to that in untreated neurons (Fig. 4A, dotted gray line, retraced from Fig. 1A to facilitate comparison). However, the slow rising phase in the later stage of the ATP/ADP ratio drop (Fig. 4A, dashed gray line) was

absent. Oligomycin addition after ER depletion did not further affect the ATP/ADP ratio of neurons stimulated with 10 mM K⁺. In contrast, depletion of Ca²⁺ from the ER did not affect the LTCC-mediated induction of RMO of ATP synthase. 10 mM K⁺ + BayK elicited a similar response in untreated neurons (Fig. 4B, dotted gray line, retraced from Fig. 1A) and thapsigargin-treated neurons (Fig. 4B, orange trace) and oligomycin evoked similar increases in the ATP/ADP ratio in both sets of neurons. Statistical evaluation revealed that the changes in ATP/ADP ratio (ADP/ATP) were significantly different between untreated and thapsigargin-treated neurons when exposed to 10 mM K⁺ (Fig. 4C, black symbols), but not when exposed to 10 mM K⁺ + BayK (Fig. 4C, gray symbols). These findings indicated that LTCC-mediated potentiation of mitochondrial ATP synthesis relied on ER-mediated Ca²⁺ release, whereas induction of RMO was CICR-independent and must involve an alternative mechanism. Another regulatory molecule that is involved in LTCC-dependent signaling in hippocampal neurons and that affects mitochondrial function is nitric oxide (NO) (33, 34). We studied the involvement of NO with L-NAME, a non-selective inhibitor of NO synthases (NOS). Pre-incubation with L-NAME appeared to reduce the initial drop in ATP/ADP ratio caused by 10 mM K⁺ (Fig. 4D, orange trace), but the decrease in the ATP/ADP ratio by oligomycin was still present. However, inhibition of NO production prevented the LTCC-mediated induction of RMO of the mitochondrial ATP synthase. In L-NAME-treated neurons, the initial drop in ATP/ADP ratio caused by 10 mM K⁺ + BayK was smaller (Fig. 4E, orange trace) than in untreated neurons (Fig. 4E, dotted gray line, retraced from Fig. 1A). Subsequent addition of oligomycin further decreased the ATP/ADP ratio in L-NAME-treated neurons, in contrast to the increase in untreated cells. Thus, 10 mM K⁺ + BayK, which induced RMO of ATP synthase in untreated neurons with functional NO synthases, enhanced mitochondrial ATP production in neurons in which NO formation was inhibited. Accordingly, oligomycin-induced changes in ATP/ADP ratio were significantly different between untreated and L-NAME-treated neurons when stimulated with 10 mM K⁺ + BayK (Fig. 4F, gray symbols), but were similar when stimulated with 10 mM K⁺ (Fig. 4F, black symbols). Hence, the potentiation of mitochondrial ATP production did not rely on a signaling cascade involving NO, unlike induction of RMO.

The production of NO in our experiments was confirmed by using the genetically encoded NO indicators geNOps targeted either to the cytosol (G-geNOp, fig. S1E) or to mitochondria (mtO-geNOp, fig. S1F) (35). The fluorescence of these sensors is quenched by NO, which enables the monitoring of its production, whereas an increase in indicator fluorescence represents a decrease in NO concentration. Cytosolic NO was increased by 10 mM K⁺ (Fig. 5A, blue trace) and 10 mM K⁺ + BayK (Fig. 5B, blue trace) in a similar manner.

Mitochondrial NO, in contrast, was increased by 10 mM K⁺ + BayK (Fig. 5B, red trace), but not by 10 mM K⁺ (Fig. 5A, red trace). Thus, the switch of ATP synthase to RMO that was elicited by combining BayK with 10 mM K⁺ (Fig. 1A, compare black and green traces) was accompanied by rises in mitochondrial NO, whereas cytosolic NO was not affected by this facilitation of LTCC activity. When LTCC-mediated Ca²⁺ influx was inhibited by isradipine during 10 mM K⁺-stimulation, both cytosolic and mitochondrial NO were unchanged (Fig. 5C). However, profound changes in geNOp fluorescence did occur upon application of glutamate (note that these experiments were performed in the presence of isradipine to prevent depolarization-induced, secondary activation of LTCCs). Glutamate induces large

increases in NO formation, and NO is involved in glutamate-mediated excitotoxicity (36). Glutamate (100 μ M) evoked a pronounced increase in cytosolic NO (Fig. 5D, blue trace) which was followed by rises in mitochondrial NO after a delay of about 140 seconds (Fig. 5D, red trace). After 10 minutes of glutamate exposure, both probes indicated comparable increases in NO concentrations.

Our data indicated that cytosolic Ca^{2+} rises triggered by LTCC-mediated Ca^{2+} influx (activated by 10 mM K^+) and augmented by CICR could promote mitochondrial ATP synthesis. On the other hand, pronounced Ca^{2+} rises through LTCCs (activated by 10 mM K^+ + BayK) appeared to induce a switch in the operation mode of ATP synthase in a different, possibly more direct manner. To evaluate this notion, we simultaneously monitored mitochondrial Ca^{2+} ($[\text{Ca}^{2+}]_{\text{mt}}$) using CEPIA2mt and the Ca^{2+} concentration in the ER ($[\text{Ca}^{2+}]_{\text{er}}$) using CEPIA1er (fig. S1H, fig. S1I). Stimulation with 10 mM K^+ led to slow mitochondrial Ca^{2+} rises that were paralleled by decreases in Ca^{2+} in the ER (Fig. 6A). Pre-treatment of neurons with thapsigargin to deplete ER Ca^{2+} stores prevented the mitochondrial Ca^{2+} elevation (Fig. 6B, black trace; the dotted gray line retraces the response shown in red in Fig. 6A). In contrast, transient Ca^{2+} elevations in the mitochondria evoked by 10 mM K^+ + BayK were not accompanied by a reduction in Ca^{2+} in the ER (Fig. 6C) and were not abolished by pre-treatment of the neurons with thapsigargin (Fig. 6D). These findings suggested that increases in $[\text{Ca}^{2+}]_{\text{mt}}$ triggered by 10 mM K^+ did not occur directly from the plasmalemmal Ca^{2+} source (LTCCs), but from a source located at the endoplasmic reticulum. However, this ER Ca^{2+} source was not required for rises in $[\text{Ca}^{2+}]_{\text{mt}}$ elicited by 10 mM K^+ + BayK. Hence, rises in $[\text{Ca}^{2+}]_{\text{mt}}$ elicited by stimulation with either 10 mM K^+ or 10 mM K^+ + BayK could be distinguished by the origin of the Ca^{2+} fluxes and by differences in their kinetics.

A conspicuous difference between effects of 10 mM K^+ and 10 mM K^+ + BayK was seen with respect to mitochondrial NO concentrations (Fig. 5, A to D). Pre-treatment with the NOS inhibitor L-NAME transformed the relatively short-lived mitochondrial Ca^{2+} rises elicited by 10 mM K^+ + BayK into more persistent Ca^{2+} elevations (Fig. 6E, green trace). A similar change was caused by a pre-treatment with cyclosporine A, an immunosuppressant that is widely used to inhibit a mitochondrial permeability transition pore (mPTP) (37) (Fig. 6F, green trace). These results imply a role for a cyclosporine A-sensitive Ca^{2+} efflux component in generating the transient nature of mitochondrial Ca^{2+} signals. Furthermore, they suggest that NO - in addition to its role in the induction of RMO - is also involved in the mechanisms causing the transience of the 10 mM K^+ + BayK-induced mitochondrial Ca^{2+} rises.

Discussion

Mitochondria are critical determinants of cell viability and their function depends on Ca^{2+} -signaling, both in the cytosol and in the mitochondrial matrix (19, 38). Influx through LTCCs is a crucial source of Ca^{2+} elevations in the cytosol as well as within mitochondria (17). Hence, the role of LTCC in neuronal survival may crucially depend on the impact of LTCC-mediated Ca^{2+} influx on mitochondria.

In this study, we report on dual effects of LTCC-mediated Ca^{2+} influx on mitochondrial ATP production, which was assayed with the ATP synthase inhibitor oligomycin and a fluorescence indicator of the ATP/ADP ratio. Our results can be summarized as follows. When neuronal activity is low (for example in unstimulated neurons, represented by the schematic neuronal membrane potential recording), the mitochondrially-generated pool of ATP is small. The major fraction of ATP is provided by glycolysis (Fig. 7A). With an increase in neuronal activity (for example, upon stimulation with 10 mM K^+ in our experiments), concomitant LTCC-mediated Ca^{2+} influx (Fig. 7B) triggers the release of Ca^{2+} from the endoplasmic reticulum (ER) Ca^{2+} store (a process known as CICR) (Fig. 7C), which also leads to Ca^{2+} rises in the vicinity of mitochondria, in particular where these organelles come in close contact at “mitochondria-associated membranes” (MAMs) (Fig. 7D). Locally, Ca^{2+} may stimulate mitochondrial respiration from outside the mitochondria by increasing the import of metabolites through Ca^{2+} -sensitive mitochondrial carrier proteins (MCP) (39) that are subsequently used for regeneration of respiratory substrates such as reduced nicotinamide adenine dinucleotide (NADH) (Fig. 7E). Ca^{2+} -dependent stimulation of mitochondrial respiration may also arise intra-mitochondrially from a direct stimulation of several enzymes in the tricarboxylic acid (TCA) cycle, such as pyruvate dehydrogenase (PDH), isocitrate dehydrogenase (IDH) and α -ketoglutarate dehydrogenase (α -KGD) (Fig. 7F). Increased mitochondrial respiration leads to increased proton extrusion by the electron transport chain (ETC) (Fig. 7G), which provides a large driving force for ATP synthase operating in forward mode (Fig. 7H). Consequently, mitochondrial ATP formation increases. During pronounced neuronal activity-dependent depolarizations (for example, upon stimulation with 20 mM K^+ or 10 mM K^+ + BayK in our experiments), large increases in cytosolic Ca^{2+} mediated by LTCC activation lead to a steep rise in mitochondrial Ca^{2+} (Fig. 7I) and activation of mitochondria-associated nitric oxide synthase (NOS) (Fig. 7J) which generates nitric oxide (NO) (Fig. 7K). At the same time, the operational mode of the ATP synthase reverses, so that mitochondria hydrolyze ATP instead of producing it (Fig. 7L). ATP synthase operating in reverse mode likely counterbalances the elevation of mitochondrial Ca^{2+} by pumping protons from the mitochondrial matrix to the intermembrane space, thus increasing the H^+ driving force for Na^+ extrusion. In turn, this effect would provide a Na^+ transmembrane gradient required for the extrusion of Ca^{2+} by the mitochondrial $\text{Na}^+/\text{Ca}^{2+}$ exchanger (NCLX) (Fig. 7M). However, a major component of the Ca^{2+} extrusion pathway was sensitive to inhibition by cyclosporine A. Hence, mPTP opening (Fig. 7N) cannot be ruled out at present as a contributing mechanism to the rapid termination of potentially deleterious mitochondrial Ca^{2+} surges.

The LTCC-dependent stimulation of mitochondrial ATP production was not mimicked by glutamate-induced cytosolic Ca^{2+} elevations, which indicates source-specificity. This was evidenced by a lack of effect of oligomycin on the ATP/ADP ratio during the application of 10 μM glutamate, for which we had also expected a further drop in the ATP/ADP ratio (Fig. 1E). Our results suggested that the endoplasmic reticulum and CICR might provide this source specificity, because depletion of ER Ca^{2+} content abolished the stimulatory action of 10 mM K^+ on mitochondrial ATP synthesis (Fig. 4A). The LTCC-mediated Ca^{2+} influx that promoted mitochondrial ATP production (as evidenced by the isradipine-sensitivity of this effect) was small in measurements of cytosolic Ca^{2+} rises (Fig. 1F). However, mitochondria

can be positioned in close proximity to Ca^{2+} release sites of the ER (for example, at “MAMs”) (40)). Hence, a considerable fraction of the Ca^{2+} signal elicited by 10 mM K^+ in the micro-environment may have escaped detection by our cytosolic Ca^{2+} indicator, although being large enough to affect mitochondrial function locally. Indeed, mitochondrial carrier proteins required for metabolite transport can be activated by modest increases in $[\text{Ca}^{2+}]_{\text{cyt}}$ not much above baseline (19). Furthermore, Ca^{2+} -sensitive mitochondrial carrier proteins contain high affinity, EF-hand Ca^{2+} binding motifs (39).

The current knowledge regarding mechanisms leading to ATP synthase reversal is fragmentary (41). In principle, the mode of operation is understood to be governed by the reversal potential of the ATP synthase ($E_{\text{rev-ATPase}}$, (42)). Accordingly, induction of RMO has been ascribed to mitochondrial depolarization beyond $E_{\text{rev-ATPase}}$ (43). However, in our study, neurons treated with 10 mM K^+ + BayK showed hyperpolarization of the mitochondrial membrane potential rather than a depolarization (Fig. 2A, green trace), despite a considerable initial mitochondrial Ca^{2+} load (Fig. 3A). Theoretically, this might be related to an increase in respiration by Ca^{2+} -dependent uptake of substrates and reducing equivalents. Nevertheless, the observed hyperpolarization was directly maintained by the ATP synthase, as revealed by pre-application of oligomycin, which prevented any hyperpolarization and instead led to a depolarization of Ψ_{mt} . As noted above, the activation of RMO requires a change in Ψ_{mt} beyond the $E_{\text{rev-ATPase}}$, which is about 10 to 15 mV more positive than the average membrane potential of resting mitochondria (43). However, modelling studies have demonstrated that $E_{\text{rev-ATPase}}$ can shift considerably to more polarized potentials upon changes in contributing parameters, such as a drop in the free phosphate concentration in the mitochondrial matrix or a reduction of the H^+/ATP coupling ratio (42). Future research, likely using isolated mitochondria, will be required to determine which of these reversal potential-determining parameters may probably change upon LTCC-mediated Ca^{2+} rises. ATP synthase reversal was accompanied by NO formation, presumably by mitochondria-associated (although not necessarily mitochondrially located) NO synthase (44) and inhibition of NO synthase with L-NAME prevented ATP synthase reversal. These data suggested that NO represents a crucial signaling molecule in the LTCC-dependent reversal of ATP synthase operating mode. However, the exact signaling pathway that may connect LTCC-mediated Ca^{2+} influx to the induction of reverse mode operation of the ATP synthase and the role of NO need to be elucidated.

Changes in TMRM fluorescence of a similar order of magnitude as in our study have been observed in other living cells upon oligomycin application or various other treatments (45–49). In addition, Li et al. (45) performed a calibration of Ψ_{mt} and calculated that their 2.5 fold increase of TMRM fluorescence induced by oligomycin corresponded to a hyperpolarization of Ψ_{mt} by about 25 mV. Moreover, Ψ_{mt} in intact neurons displays considerable variability, and cultured rat cortical neurons show a range of -108 mV to -158 mV (50). Similar Ψ_{mt} values have been determined in non-neural cells (45), and the mechanisms underlying the differences in Ψ_{mt} between living organisms and isolated mitochondria (beyond -180 mV) have been described (51).

Like NMDA-type glutamate receptor-mediated Ca^{2+} influx, sustained Ca^{2+} entry through LTCCs has also been suggested to cause mitochondrial Ca^{2+} -overload, organelle dysfunction

and subsequently activation and release of apoptotic cascade mediators (14). However, our results demonstrated that LTCC-dependent mitochondrial Ca^{2+} elevations were transient even in the presence of continuous LTCC-mediated Ca^{2+} influx (Fig. 1F, green trace) and could thus be repeated several times in a neuron during conditions associated with RMO of the ATP synthase (Fig. 3D). On the other hand, a persistent accumulation of $[\text{Ca}^{2+}]_{\text{mt}}$ occurred during the stimulation with 30 to 100 μM glutamate (Fig. 3E), which did not lead to induction of ATP synthase reversal. We do not know yet whether a mechanistic relation exists between ATP synthase reversal and the early termination of the mitochondrial Ca^{2+} rise, or whether they are independent processes aimed to protect mitochondria. ATP synthase has been molecularly linked to a mPTP (52), but there is doubt that subunits of the ATP synthase form the mitochondrial transition pore (53). In our experiments (Fig. 6, E and F), the transient mitochondrial Ca^{2+} response was turned into a persistent Ca^{2+} elevation by inhibition of NOS with L-NAME and by cyclosporine A, which exerts inhibitory activity on mPTP (37), but probably also on NOS (54), although the later effect on NOS is not seen consistently (55). Because NO is a modulator of mPTP (56, 57), LTCC-dependent Ca^{2+} elevations in the mitochondria may stimulate a mitochondria-associated NOS. Thus, NO formation may lead to the activation of the mPTP, but this would need to be transient in nature, because we did not see strong mitochondrial depolarization (although brief depolarizations could have been missed by the slowly redistributing indicator dye). In addition, we did not observe concomitant cell death that has been reported for mPTP, such as that associated with glutamate excitotoxicity (58). However, there may be physiological roles of mPTP, as has been proposed for the regulation of mitochondrial Ca^{2+} in cortical neurons (59). Alternatively, another cyclosporine A-sensitive Ca^{2+} extrusion mechanism, which does not rely on mPTP, has been described in non-neuronal cells (60). It remains unclear if such a mechanism also exists in neurons. Other Ca^{2+} efflux systems, such as the mitochondrial $\text{Na}^+/\text{Ca}^{2+}$ exchanger (NCLX, (61)) represent additional candidates for terminating $[\text{Ca}^{2+}]_{\text{mt}}$ rises.

At present, it remains under debate how stimulation of ATP synthase activity and reverse mode operation of ATP synthase may impinge on neuronal viability. LTCC-dependent stimulation of the mitochondrial ATP production may improve the ability of the neurons to cope with enhanced energy demands, such as in fueling pumps required for the maintenance of electrolyte homeostasis. Likewise, a beneficial cytoprotective effect of ATP synthase RMO, which also involves mitochondrial hyperpolarization, has been demonstrated for T cell leukemia cells and for astrocytes, but not for embryonic cortical neurons (62, 63). Moreover, cortical neurons differentiated in vitro from induced pluripotent stem cells from neurodegenerative disease patients show ATP synthase reversal, but this was linked to increased cell death (64). In contrast, we showed that RMO of ATP synthase was associated with maintenance or hyperpolarization of Ψ_{mt} and did not lead to hippocampal neuronal death within a 30-hour observational period (Fig. 3F). The cause of this discrepancy remains unknown. Increased cell death upon RMO has been explained by excess ROS formation in the hyperpolarized mitochondria (64) or ATP loss. However, considerations regarding the probable supply rate of extra-mitochondrial ATP actually argue against a rapid depletion of ATP (43). Hence, the induction of RMO (Fig. 7L) may alternatively reflect a temporarily successful attempt to use available ATP (glycolytically-generated or provided by

mitochondrial substrate-level phosphorylation (65, 66) to mitigate mitochondrial damage. This effect may be achieved by repurposing ATP to maintain the proton gradient that is necessary for electrolyte balance across the inner mitochondrial membrane (67). We have no data yet on the persistence of this mechanism, but we envisage that it may come with unsustainable costs if cellular crisis continues.

In conclusion, our study revealed a LTCC-mediated, source-specific Ca^{2+} regulation of mitochondrial function. Regardless of the precise mechanisms involved in this regulation, our results suggest that attempts to employ LTCC inhibitors for neuroprotection efforts should thus consider the possibility that LTCC-mediated Ca^{2+} influx may contribute to the tuning of mitochondrial ATP production to energetic neuronal needs and that it may also play a crucial role in the acute maintenance of mitochondrial function during unfavorable conditions.

Materials and Methods

Primary cell culture of hippocampal neurons

Pregnant Sprague-Dawley rats were provided by the Department of Biomedical Research, Division for Laboratory Animal Science and Genetics, Himberg, Austria. Neonatal animals were killed by decapitation in full accordance with all rules of the Austrian animal protection law (see http://www.ris.bka.gv.at/Dokumente/BgblAuth/BGBLA_2012_I_114/BGBLA_2012_I_114.pdf) and the Austrian animal experiment by-laws (see http://www.ris.bka.gv.at/Dokumente/BgblAuth/BGBLA_2012_II_522/BGBLA_2012_II_522.pdf) which implement European (DIRECTIVE 2010/63/EU; see <http://eurlex.europa.eu/LexUriServ/LexUriServ.do?uri=OJ:L:2010:276:0033:0079:en:PDF>) into Austrian law (all information accessed on August 30th, 2019). The responsible animal welfare body is the “Ethics Committee of the Medical University of Vienna for Research Projects Involving Animals”. Brains were removed to dissect the hippocampi in ice-cold buffer which contained (in mM): 137 NaCl, 5.4 KCl, 1.1 Na_2HPO_4 , 1.1 KH_2PO_4 , 6.1 glucose, and 1 kynurenic acid, and in which pH was adjusted to 7.3 with NaOH. (68). Primary co-cultures of hippocampal neurons and glial cells were prepared after enzymatic digestion of brain tissue for 20 minutes at $37^\circ\text{C}/5\% \text{CO}_2$ with papain (LS003124, Worthington) at a concentration of 25 units/ml in L-15 Leibovitz medium (L5520, Sigma-Aldrich) supplemented with 2 mM kynurenic acid (K3375, Sigma-Aldrich) and mechanical dissociation with Pasteur pipettes (trituration). The culture medium used was based on Dulbecco’s Modified Eagle’s Medium - high glucose (D5796, Sigma-Aldrich) supplemented with 10% γ -irradiated fetal bovine serum (S 0415, Biochrom), 12.5 nM progesterone (P8783, Sigma-Aldrich), 112.5 μM putrescine dihydrochloride (P5780, Sigma-Aldrich) and 6.25 $\mu\text{g}/\text{ml}$ insulin, 6.25 $\mu\text{g}/\text{ml}$ transferrin, 6.25 ng/ml sodium selenite (added from a 400-times concentrated stock solution of Insulin-Transferrin-Sodium Selenite Supplement, Roche 11 074 547 001). The medium also contained 25,000 U/l penicillin and 25 mg/l streptomycin, which was added from a 400-times concentrated stock (P4333, Sigma-Aldrich). From the final single cell suspension, we seeded 50,000 cells into microchambers ($\sim 45 \text{ mm}^2$) created by glass rings positioned in the center of 35 mm diameter culture dishes, which were either from Thermo Fisher Scientific (153066) or from MatTek Corporation for

imaging experiments. Glass rings were removed 2 hours after seeding. The initial medium was exchanged after 24 h for the same medium but without antibiotics. 1 μM cytosine arabinoside (C6645, Sigma-Aldrich) was added at day 3 to 4 after the preparation to reduce the proliferation of non-neuronal cells. Neurons were cultured for at least 12 days at 37°C and 5% CO_2 before experiments were performed. To compensate for evaporation from the medium during that time, 200 μl autoclaved and sterile filtered purified water was added once a week.

Drugs and Chemicals

Final concentration used in the experiments is indicated in parentheses preceding the compound's name. (500 $\mu\text{g/ml}$) Amphotericin B (A4888, from *Streptomyces* sp.), (3 μM) Bay K8644 (B112), (1 and 10 μM) bicuculline methiodide (14343), (10 μM) 1,2-Bis(2-aminophenoxy)ethane-*N,N,N',N'*-tetraacetic acid tetrakis(acetoxymethyl ester) (BAPTA-AM, A1076), (10 μM) diltiazem (D2521), (0.03%) dimethyl sulfoxide (DMSO, D2650), (1 μM) carbonyl cyanide 4-(trifluoromethoxy)phenylhydrazone (FCCP, C2920), (10, 30, 100 μM) glutamate (G1251), (3 μM) isradipine (I6658), (100 μM) N_ω -Nitro-L-arginine methyl ester hydrochloride (L-NAME, N5751), (2 μM) oligomycin (O4876), (20 μM) propidium iodide (P4170), (2 μM) thapsigargin (T9033) and bulk chemicals were purchased from Sigma-Aldrich. (1 μM) Cyclosporine A (12088) was from Cayman Chemical. Isradipine and Bay K8644 were dissolved from 10 mM stock solutions in DMSO to a final concentration of 3 μM in aqueous buffer. Hence, 0.03% DMSO was also added to the respective control solutions. For some experiments, the cells were pre-treated either in the incubator (37°C/5% CO_2) for 45 minutes (BAPTA-AM) and 30 minutes (L-NAME), or at room temperature for 15 minutes (thapsigargin) and 10 minutes (cyclosporine A) by adding the respective compounds to the external solution. Except for BAPTA-AM, compounds were then also present at the same concentrations in the external solutions used for superfusion of the cells in the electrophysiological or imaging experiments.

Transfections

Transfections were performed using Lipofectamine 2000 reagent (Invitrogen, Thermo Fisher Scientific) according to the manufacturer's instructions with some modifications. In brief, neuronal cultures older than 12 days-in-vitro (DIV) were incubated in 500 μL of antibiotic-free medium containing 3 μL of Lipofectamine and 1.5 μg of plasmid DNA for 3 hours. The transfection medium was replaced with original medium and the neurons were kept for 3 days in the incubator. Experiments were performed on day 3 after transfection.

Electrophysiology

Membrane voltage was recorded using a Multiclamp 700B amplifier (Axon Instruments) in the current clamp mode using Clampex 10.5 software, which is part of the pCLAMP 10 electrophysiology data acquisition and analysis software package (Molecular Devices). Signals were low-pass filtered at 10 kHz and were digitized with a Digidata 1440A digitizer (Molecular Devices) at a sampling rate of 20 kHz. Patch pipettes were made of borosilicate capillaries (GB150-8P, Science Products) with a Sutter P97 horizontal puller (Sutter Instrument Company). Tip resistances were between 3.5 and 5 M Ω . The pipette solution was composed of (in mM) 120 potassium gluconate, 1.5 sodium gluconate, 3.5 NaCl, 1.5 CaCl_2 ,

0.25 MgCl₂, 10 HEPES, and 5 EGTA. pH was adjusted to 7.3 by KOH. All recordings were made in perforated patch mode using the antimycotic compound amphotericin B, which was added to the pipette solution just before experiments. The amphotericin B pipette solution was used to back-fill the patch pipette after the pipette tip had been filled by capillary force with the same solution but not containing the antimycotic compound to enable better seal formation. After seal formation, experiments were started only when the series resistance had dropped to the lowest achievable level (between 20 and 30 MΩ), which usually required 15 minutes. To ensure that only viable cells were used, the following inclusion criteria had to be met: a membrane voltage of at least -50 mV and the capability of generating overshooting action potentials, which was always tested prior to recording. Experiments were performed at room temperature (22-24° C), and cells were superfused continuously using a DAD-12 drug application system (Adams & List) with a micromanifold that held 12 channels converging into a 100 μm diameter quartz outlet. The tip of the outlet was positioned in close proximity (about 250 μm) to the patch-clamped cell. The external solution was composed of (in mM): 140 NaCl, 3 KCl, 2 CaCl₂, 2 MgCl₂, 10 HEPES, 20 glucose (pH was adjusted to 7.4 by NaOH). The concentration of KCl in the test solutions (referred to as 10 K⁺, 20 K⁺ and 30 K⁺) was adjusted to 10, 20 or 30 mM. All solutions were osmotically balanced by lowering the NaCl content. Test compounds were added to external solution and were superfused from reservoirs connected to one of the 12 micromanifold channels.

Imaging

For imaging purposes, neurons and glial cells were co-cultured in glass bottom dishes (P35GC-1.5-14-C, MatTek Corporation). Before each experiment, the culturing medium was replaced by external solution. Experiments were performed at room temperature, and cells were superfused continuously using an 8-reservoir drug application system (Octaflow II) with a micromanifold that held 8 channels converging into a 100 μm diameter quartz outlet. Neurons were imaged using Nikon AIR confocal microscope equipped with a focus clamp. Representative micrographs of neurons expressing or loaded with the various fluorescence sensors used in this study are shown in fig. S1, A to I.

The ATP/ADP ratio was determined in neurons expressing the genetically encoded fluorescence sensor PercevalHR (referred to as “Perceval”), with excitation at 403 nm and 488 nm wavelengths while the emission was detected at 525 nm. The quotient F_{488}/F_{403} reflects the intraneuronal ATP/ADP ratio. The expression vector GW1-PercevalHR was a gift from Gary Yellen (Addgene plasmid # 49082) (26). Cytosolic pH was monitored using the genetically encoded indicator GW1-pHRed (Addgene plasmid #31473) (69), with excitation/emission wavelengths of 562/595 nm.

Intracellular Ca²⁺ ([Ca²⁺]_{cyt}) was measured using Fluo-4 AM (F14201, Invitrogen, Thermo Fisher Scientific). Neurons were incubated for 15 minutes at 37 °C in 1 μM Fluo-4 AM-containing buffer solution followed by a washout with extracellular solution. Neurons were excited by 488 nm and emission was detected at 525 nm.

Mitochondrial Ca²⁺ ([Ca²⁺]_{mt}) was measured using the genetically encoded fluorescence sensor CEPIA2mt. The expression vector pCMV CEPIA2mt was a gift from Masamitsu Iino

(Addgene plasmid # 58218) (70). Excitation/emission wavelengths for experiments with CEPIA2mt were 488/525 nm.

Ca²⁺ in the endoplasmic reticulum ([Ca²⁺]_{er}) was measured using the genetically encoded fluorescence sensor CEPIA1er. The expression vector pCMV R-CEPIA1er was a gift from Masamitsu Iino (Addgene plasmid # 58216) (70). Excitation/emission wavelengths for experiments with CEPIA1er were 562/595 nm. For the experiments in Fig. 6, A and C, both CEPIA sensors were co-expressed.

To measure mitochondrial membrane potential (Ψ_{mt}) with TMRM (T668, Invitrogen, Thermo Fisher Scientific), cultures were equilibrated for 1 hour in 1 nM TMRM at 37 °C. The incubation period was not followed by a washout and the dye was present in all perfusing solutions. Neurons were excited at 562 nm and emissions were detected at 595 nm. The terms hyperpolarization and depolarization of Ψ_{mt} were defined as any increase or decrease of the TMRM fluorescence relative to the value prior to the application of test solutions or compounds.

Monitoring of mitochondrial dynamics was performed using the genetically encoded fluorescent dye “mito-DsRed”. The expression vector mitochondrial pDsRed2 (632421) was from Clontech. Excitation/emission wavelengths for experiments with mito-DsRed were 562/595 nm.

Measurements of cytosolic and mitochondrial nitric oxide (NO) were performed using the simultaneously expressed genetically encoded fluorescence probes G-geNOp and mtO-geNOp, respectively (Next Generation Fluorescence Imaging) (35). Prior to the imaging experiments, the cells were preincubated with Fe²⁺-loading buffer for 20 minutes to fully activate the NO sensors (71). Excitation/emission wavelengths for experiments with G-geNOp were 488/525, and 562/595 nm for experiments with mtO-geNOp.

Data analysis

In all imaging experiments, fluorescence intensity was calculated as the mean intensity from a defined region of interest positioned around neuronal somata (fig. S1A). All fluorescence data were normalized to unity by dividing the whole trace by a representative control value from a stable region just before the application of the test solution. Averaged traces of the normalized data are displayed in the figures together with the standard error of the means (SEM). The values (ATP/ADP, Ψ_{mt}) depicted in the scatter plots (depicting means \pm SEM) were obtained by subtracting the data point preceding the application of 2 μ M oligomycin from the data point determined 8 minutes after its addition.

Propidium iodide uptake assay

Neuronal cultures were treated at 14 DIV with medium containing agents inducing reverse mode operation of ATP synthase or glutamate. Neurons were then left for 30 hours in the incubator. After the incubation, media were removed and neurons were treated with external solution containing propidium iodide (PI). Neurons were imaged and PI-positive neurons were counted and divided by the total number of neurons in the same field of view. The total number of neurons in the field of view was obtained from transmission light images, which

also enabled us to exclude glial cells. The ratio of PI-positive neurons versus the total number of neurons is referred to as neuronal death.

Statistics

GraphPad Prism version 7.04 was used to prepare graphs and to perform statistical testing on the assumption of normally distributed data. All statistically significant differences are labeled with asterisks which are defined in the figure legends. Statistically non-significant differences (P values > 0.05) are not separately designated in the figures.

Supplementary Material

Refer to Web version on PubMed Central for supplementary material.

Acknowledgements

We thank Gabriele Gaupmann for excellent technical assistance. We are indebted to Christos Chinopoulos (Semmelweis University, Budapest) for helpful discussions, in particular regarding ATP synthase reversal.

Funding

This work was supported by a grant of the Austrian Science Fund (FWF, project P28179) as well as by the Herzfelder'sche Familienstiftung, both to H.K.

Data and materials availability

All data needed to evaluate the conclusions in the paper are present in the paper or the Supplementary Materials. The following plasmids require a material transfer agreement from Addgene: GW1-PercevalHR, GW1-pHRed, pCMV CEPIA2mt, pCMV R-CEPIA1er.

References and Notes

- Berger SM, Bartsch D. The role of L-type voltage-gated calcium channels Cav1.2 and Cav1.3 in normal and pathological brain function. *Cell Tissue Res.* 2014; 357:463–476. [PubMed: 24996399]
- Ortner NJ, Striessnig J. L-type calcium channels as drug targets in CNS disorders. *Channels.* 2016; 10:7–13. [PubMed: 26039257]
- Brewer LD, Thibault O, Staton J, Thibault V, Rogers JT, Garcia-Ramos G, Kraner S, Landfield PW, Porter NM. Increased vulnerability of hippocampal neurons with age in culture: temporal association with increases in NMDA receptor current, NR2A subunit expression and recruitment of L-type calcium channels. *Brain Res.* 2007; 1151:20–31. [PubMed: 17433272]
- Veng LM, Mesches MH, Browning MD. Age-related working memory impairment is correlated with increases in the L-type calcium channel protein alpha1D (Cav1.3) in area CA1 of the hippocampus and both are ameliorated by chronic nimodipine treatment. *Brain Res Mol Brain Res.* 2003; 110:193–202. [PubMed: 12591156]
- Thibault O, Hadley R, Landfield PW. Elevated postsynaptic [Ca²⁺]_i and L-type calcium channel activity in aged hippocampal neurons: relationship to impaired synaptic plasticity. *J Neurosci.* 2001; 21:9744–56. [PubMed: 11739583]
- Szydłowska K, Tymianski M. Cell Calcium Calcium, ischemia and excitotoxicity. *Cell Calcium.* 2010; 47:122–129. [PubMed: 20167368]
- Yagami T, Kohma H, Yamamoto Y. L-type voltage-dependent calcium channels as therapeutic targets for neurodegenerative diseases. *Curr Med Chem.* 2012; 19:4816–27. [PubMed: 22834820]
- Ortner NJ, Bock G, Dougalis A, Kharitonova M, Duda J, Hess S, Tuluc P, Pomberger T, Stefanova N, Pitterl F, Ciossek T, et al. Lower Affinity of Isradipine for L-Type Ca²⁺ Channels during

- Substantia Nigra Dopamine Neuron-Like Activity: Implications for Neuroprotection in Parkinson's Disease. *J Neurosci*. 2017; 37:6761–6777. [PubMed: 28592699]
9. Horn J, Limburg M. Calcium antagonists for acute ischemic stroke. *Cochrane database Syst Rev*. 2000
 10. Lyden P, Wahlgren NG. Mechanisms of action of neuroprotectants in stroke. *J Stroke Cerebrovasc Dis*. 2000; 9:9–14. [PubMed: 17895214]
 11. Zhang J, Yang J, Zhang C, Jiang X, Zhou H, Liu M. Calcium antagonists for acute ischemic stroke. *Cochrane database Syst Rev*. 2012
 12. Li X-M, Yang J, Hu D-H, Hou F, Zhao M, Zhu X, Wang Y, Li J, Hu P, Chen L, Qin L, et al. Contribution of downregulation of L-type calcium currents to delayed neuronal death in rat hippocampus after global cerebral ischemia and reperfusion. *J Neurosci*. 2007; 27:5249–59. [PubMed: 17494711]
 13. Hu H, Li S, Wang P, Yan H, Cao X, Hou F, Fang Y, Zhu X, Gao T. An L-type calcium channel agonist, bay K8644, extends the window of intervention against ischemic neuronal injury. *Mol Neurobiol*. 2013; 47:280–9. [PubMed: 23054684]
 14. Cano-Abad MF, Villarroya M, García AG, Gabilan NH, López MG. Calcium entry through L-type calcium channels causes mitochondrial disruption and chromaffin cell death. *J Biol Chem*. 2001; 276:39695–704. [PubMed: 11500491]
 15. Stanika RI, Pivovarova NB, Brantner CA, Watts CA, Winters CA, Andrews SB. Coupling diverse routes of calcium entry to mitochondrial dysfunction and glutamate excitotoxicity. *Proc Natl Acad Sci U S A*. 2009; 106:9854–9. [PubMed: 19482936]
 16. Surmeier DJ, Guzman JN, Sanchez-Padilla J, Schumacker PT. The role of calcium and mitochondrial oxidant stress in the loss of substantia nigra pars compacta dopaminergic neurons in Parkinson's disease. *Neuroscience*. 2011; 198:221–31. [PubMed: 21884755]
 17. Stanika RI, Villanueva I, Kazanina G, Andrews SB, Pivovarova NB. Comparative impact of voltage-gated calcium channels and NMDA receptors on mitochondria-mediated neuronal injury. *J Neurosci*. 2012; 32:6642–50. [PubMed: 22573686]
 18. Pivovarova NB, Andrews SB. Calcium-dependent mitochondrial function and dysfunction in neurons. *FEBS J*. 2010; 277:3622–36. [PubMed: 20659161]
 19. Llorente-Folch I, Rueda CB, Pardo B, Szabadkai G, Duchon MR, Satrustegui J. The regulation of neuronal mitochondrial metabolism by calcium. *J Physiol*. 2015; 593:3447–62. [PubMed: 25809592]
 20. Kann O, Kovács R. Mitochondria and neuronal activity. *Am J Physiol Cell Physiol*. 2007; 292:C641–57. [PubMed: 17092996]
 21. Galli C, Meucci O, Scorziello A, Werge T, Calissano P, Schettini G. Apoptosis in cerebellar granule cells is blocked by high KCl, forskolin, and IGF-1 through distinct mechanisms of action: the involvement of intracellular calcium and RNA synthesis. *J Neurosci*. 1995; 15:1172–1179. [PubMed: 7532699]
 22. Tongiorgi E, Righi M, Cattaneo A. Activity-Dependent Dendritic Targeting of BDNF and TrkB mRNAs in Hippocampal Neurons. *J Neurosci*. 1997; 17:9492–9505. [PubMed: 9391005]
 23. Brosenitsch TA, Salgado-Commissariat D, Kunze DL, Katz DM. A Role for L-Type Calcium Channels in Developmental Regulation of Transmitter Phenotype in Primary Sensory Neurons. *J Neurosci*. 1998; 18:1047–1055. [PubMed: 9437025]
 24. Li J, Kato K, Ikeda J, Morita I, Murota SI. A narrow window for rescuing cells by the inhibition of calcium influx and the importance of influx route in rat cortical neuronal cell death induced by glutamate. *Neurosci Lett*. 2001; 304:29–32. [PubMed: 11335047]
 25. Duberley KEC, Abramov AY, Chalasani A, Heales SJ, Rahman S, Hargreaves IP. Human neuronal coenzyme Q10 deficiency results in global loss of mitochondrial respiratory chain activity, increased mitochondrial oxidative stress and reversal of ATP synthase activity: implications for pathogenesis and treatment. *J Inherit Metab Dis*. 2013; 36:63–73. [PubMed: 22767283]
 26. Tantama M, Martínez-François JR, Mongeon R, Yellen G. Imaging energy status in live cells with a fluorescent biosensor of the intracellular ATP-to-ADP ratio. *Nat Commun*. 2013; 4:2550. [PubMed: 24096541]

27. Oliveira JMA. Techniques to investigate neuronal mitochondrial function and its pharmacological modulation. *Curr Drug Targets*. 2011; 12:762–73. [PubMed: 21275887]
28. Perry SW, Norman JP, Barbieri J, Brown EB, Gelbard HA. Mitochondrial membrane potential probes and the proton gradient: a practical usage guide. *Biotechniques*. 2011; 50:98–115. [PubMed: 21486251]
29. Gutiérrez R, Armand V, Schuchmann S, Heinemann U. Epileptiform activity induced by low Mg²⁺ in cultured rat hippocampal slices. *Brain Res*. 1999; 815:294–303. [PubMed: 9878794]
30. Orrenius S, Gogvadze V, Zhivotovsky B. Calcium and mitochondria in the regulation of cell death. *Biochem Biophys Res Commun*. 2015; 460:72–81. [PubMed: 25998735]
31. Galloway CA, Lee H, Yoon Y. Mitochondrial morphology-emerging role in bioenergetics. *Free Radic Biol Med*. 2012; 53:2218–28. [PubMed: 23032099]
32. Thibault O, Gant JC, Landfield PW. Expansion of the calcium hypothesis of brain aging and Alzheimer's disease: minding the store. *Aging Cell*. 2007; 6:307–17. [PubMed: 17465978]
33. Bustamante J, Czerniczyniec A, Lores-Arnaiz S. Brain nitric oxide synthases and mitochondrial function. *Front Biosci*. 2007; 12:1034–40. [PubMed: 17127358]
34. Pigott BM, Garthwaite J. Nitric Oxide Is Required for L-Type Ca(2+) Channel-Dependent Long-Term Potentiation in the Hippocampus. *Front Synaptic Neurosci*. 2016; 8:17. [PubMed: 27445786]
35. Eroglu E, Gottschalk B, Charoensin S, Blass S, Bischof H, Rost R, Madreiter-Sokolowski CT, Pelzmann B, Bernhart E, Sattler W, Hallström S, et al. Development of novel FP-based probes for live-cell imaging of nitric oxide dynamics. *Nat Commun*. 2016; 7:10623. [PubMed: 26842907]
36. Lau A, Tymianski M. Glutamate receptors, neurotoxicity and neurodegeneration. *Pflugers Arch*. 2010; 460:525–42. [PubMed: 20229265]
37. Hansson MJ, Persson T, Friberg H, Keep MF, Rees A, Wieloch T, Elmér E. Powerful cyclosporin inhibition of calcium-induced permeability transition in brain mitochondria. *Brain Res*. 2003; 960:99–111. [PubMed: 12505662]
38. Celsi F, Pizzo P, Brini M, Leo S, Fotino C, Pinton P, Rizzuto R. Mitochondria, calcium and cell death: a deadly triad in neurodegeneration. *Biochim Biophys Acta*. 2009; 1787:335–44. [PubMed: 19268425]
39. Gutiérrez-Aguilar M, Baines CP. Physiological and pathological roles of mitochondrial SLC25 carriers. *Biochem J*. 2013; 454:371–86. [PubMed: 23988125]
40. Rizzuto R, Marchi S, Bonora M, Aguiari P, Bononi A, De Stefani D, Giorgi C, Leo S, Rimessi A, Siviero R, Zecchini E, et al. Ca(2+) transfer from the ER to mitochondria: when, how and why. *Biochim Biophys Acta*. 2009; 1787:1342–51. [PubMed: 19341702]
41. Jonckheere AI, Smeitink JAM, Rodenburg RJT. Mitochondrial ATP synthase: architecture, function and pathology. *J Inher Metab Dis*. 2012; 35:211–25. [PubMed: 21874297]
42. Chinopoulos C. The “B Space” of mitochondrial phosphorylation. *J Neurosci Res*. 2011; 89:1897–1904. [PubMed: 21541983]
43. Chinopoulos C. Mitochondrial consumption of cytosolic ATP: not so fast. *FEBS Lett*. 2011; 585:1255–9. [PubMed: 21486564]
44. Lacza Z, Pankotai E, Busija DW. Mitochondrial nitric oxide synthase: current concepts and controversies. *Front Biosci (Landmark Ed)*. 2009; 14:4436–43. [PubMed: 19273361]
45. Li R, Beebe T, Cui J, Rouhanizadeh M, Ai L, Wang P, Gundersen M, Takabe W, Hsiai TK. Pulsatile shear stress increased mitochondrial membrane potential: implication of Mn-SOD. *Biochem Biophys Res Commun*. 2009; 388:406–12. [PubMed: 19666009]
46. Gautier CA, Giaime E, Caballero E, Núñez L, Song Z, Chan D, Villalobos C, Shen J. Regulation of mitochondrial permeability transition pore by PINK1. *Mol Neurodegener*. 2012; 7:22. [PubMed: 22630785]
47. Jin H-J, Xie X-L, Ye J-M, Li C-G. Tanshinone IIA and cryptotanshinone protect against hypoxia-induced mitochondrial apoptosis in H9c2 cells. *PLoS One*. 2013; 8:e51720. [PubMed: 23341883]
48. Forkink M, Manjeri GR, Liemburg-Apers DC, Nibbeling E, Blanchard M, Wojtala A, Smeitink JAM, Wieckowski MR, Willems PHGM, Koopman WJH. Mitochondrial hyperpolarization during chronic complex I inhibition is sustained by low activity of complex II, III, IV and V. *Biochim Biophys Acta*. 2014; 1837:1247–56. [PubMed: 24769419]

49. D'Orsi B, Kilbride SM, Chen G, Perez Alvarez S, Bonner HP, Pfeiffer S, Plesnila N, Engel T, Henshall DC, Düssmann H, Prehn JHM. Bax regulates neuronal Ca²⁺ homeostasis. *J Neurosci*. 2015; 35:1706–22. [PubMed: 25632145]
50. Gerencser AA, Chinopoulos C, Birket MJ, Jastroch M, Vitelli C, Nicholls DG, Brand MD. Quantitative measurement of mitochondrial membrane potential in cultured cells: calcium-induced de- and hyperpolarization of neuronal mitochondria. *J Physiol*. 2012; 590:2845–71. [PubMed: 22495585]
51. Kadenbach B, Ramzan R, Wen L, Vogt S. New extension of the Mitchell Theory for oxidative phosphorylation in mitochondria of living organisms. *Biochim Biophys Acta*. 2010; 1800:205–12. [PubMed: 19409964]
52. Chinopoulos C. ATP synthase complex and the mitochondrial permeability transition pore: poles of attraction. *EMBO Rep*. 2017; 18:1041–1042. [PubMed: 28630136]
53. Chinopoulos C. Mitochondrial permeability transition pore: Back to the drawing board. *Neurochem Int*. 2018; 117:49–54. [PubMed: 28647376]
54. Diaz-Ruiz A, Vergara P, Perez-Severiano F, Segovia J, Guizar-Sahagún G, Ibarra A, Ríos C. Cyclosporin-A inhibits constitutive nitric oxide synthase activity and neuronal and endothelial nitric oxide synthase expressions after spinal cord injury in rats. *Neurochem Res*. 2005; 30:245–51. [PubMed: 15895828]
55. Fujisaki Y, Yamauchi A, Dohgu S, Sunada K, Yamaguchi C, Oishi R, Kataoka Y. Cyclosporine A-increased nitric oxide production in the rat dorsal hippocampus mediates convulsions. *Life Sci*. 2002; 72:549–56. [PubMed: 12467895]
56. Brookes PS, Salinas EP, Darley-USmar K, Eiserich JP, Freeman BA, Darley-USmar VM, Anderson PG. Concentration-dependent effects of nitric oxide on mitochondrial permeability transition and cytochrome c release. *J Biol Chem*. 2000; 275:20474–9. [PubMed: 10791954]
57. Ohtani H, Katoh H, Tanaka T, Saotome M, Urushida T, Satoh H, Hayashi H. Effects of nitric oxide on mitochondrial permeability transition pore and thiol-mediated responses in cardiac myocytes. *Nitric oxide Biol Chem*. 2012; 26:95–101.
58. Almeida A, Bolaños JP. A transient inhibition of mitochondrial ATP synthesis by nitric oxide synthase activation triggered apoptosis in primary cortical neurons. *J Neurochem*. 2001; 77:676–90. [PubMed: 11299330]
59. Barsukova A, Komarov A, Hajnóczky G, Bernardi P, Bourdette D, Forte M. Activation of the mitochondrial permeability transition pore modulates Ca²⁺ responses to physiological stimuli in adult neurons. *Eur J Neurosci*. 2011; 33:831–42. [PubMed: 21255127]
60. Richter C, Schlegel J. Mitochondrial calcium release induced by prooxidants. *Toxicol Lett*. 1993; 67:119–27. [PubMed: 8451754]
61. Palty R, Silverman WF, Hershinkel M, Caporale T, Sensi SL, Parnis J, Nolte C, Fishman D, Shoshan-Barmatz V, Herrmann S, Khananshvil D, et al. NCLX is an essential component of mitochondrial Na⁺/Ca²⁺ exchange. *Proc Natl Acad Sci U S A*. 2010; 107:436–41. [PubMed: 20018762]
62. Almeida A, Almeida J, Bolaños JP, Moncada S. Different responses of astrocytes and neurons to nitric oxide: the role of glycolytically generated ATP in astrocyte protection. *Proc Natl Acad Sci U S A*. 2001; 98:15294–9. [PubMed: 11742096]
63. Beltrán B, Quintero M, García-Zaragoza E, O'Connor E, Esplugues JV, Moncada S. Inhibition of mitochondrial respiration by endogenous nitric oxide: a critical step in Fas signaling. *Proc Natl Acad Sci U S A*. 2002; 99:8892–7. [PubMed: 12077295]
64. Esteras N, Rohrer JD, Hardy J, Wray S, Abramov AY. Mitochondrial hyperpolarization in iPSC-derived neurons from patients of FTDP-17 with 10+16 MAPT mutation leads to oxidative stress and neurodegeneration. *Redox Biol*. 2017; 12:410–422. [PubMed: 28319892]
65. Díaz-García CM, Mongeon R, Lahmann C, Koveal D, Zucker H, Yellen G. Neuronal Stimulation Triggers Neuronal Glycolysis and Not Lactate Uptake. *Cell Metab*. 2017; 26:361–374.e4. [PubMed: 28768175]
66. Chinopoulos C, Gerencser AA, Mandi M, Mathe K, Töröcsik B, Doczi J, Turiak L, Kiss G, Konràd C, Vajda S, Vereczki V, et al. Forward operation of adenine nucleotide translocase during F0F1-

- ATPase reversal: critical role of matrix substratelevel phosphorylation. *FASEB J.* 2010; 24:2405–16. [PubMed: 20207940]
67. Poburko D, Santo-Domingo J, Demaurex N. Dynamic regulation of the mitochondrial proton gradient during cytosolic calcium elevations. *J Biol Chem.* 2011; 286:11672–84. [PubMed: 21224385]
68. Geier P, Lagler M, Boehm S, Kubista H. Dynamic interplay of excitatory and inhibitory coupling modes of neuronal L-type calcium channels. *Am J Physiol Cell Physiol.* 2011; 300:C937–49. [PubMed: 21228322]
69. Tantama M, Hung YP, Yellen G. Imaging intracellular pH in live cells with a genetically encoded red fluorescent protein sensor. *J Am Chem Soc.* 2011; 133:10034–7. [PubMed: 21631110]
70. Suzuki J, Kanemaru K, Ishii K, Ohkura M, Okubo Y, Iino M. Imaging intraorganellar Ca²⁺ at subcellular resolution using CEPIA. *Nat Commun.* 2014; 5:4153. [PubMed: 24923787]
71. Eroglu E, Rost R, Bischof H, Blass S, Schreilechner A, Gottschalk B, Depaoli MR, Klec C, Charoensin S, Madreiter-Sokolowski CT, Ramadan J, et al. Application of Genetically Encoded Fluorescent Nitric Oxide (NO•) Probes, the geNOps, for Real-time Imaging of NO• Signals in Single Cells. *J Vis Exp.* 2017:110.

One-sentence summary

L-type Ca^{2+} channel activity confers neuroprotection by inducing the ATP synthase to operate in reverse mode.

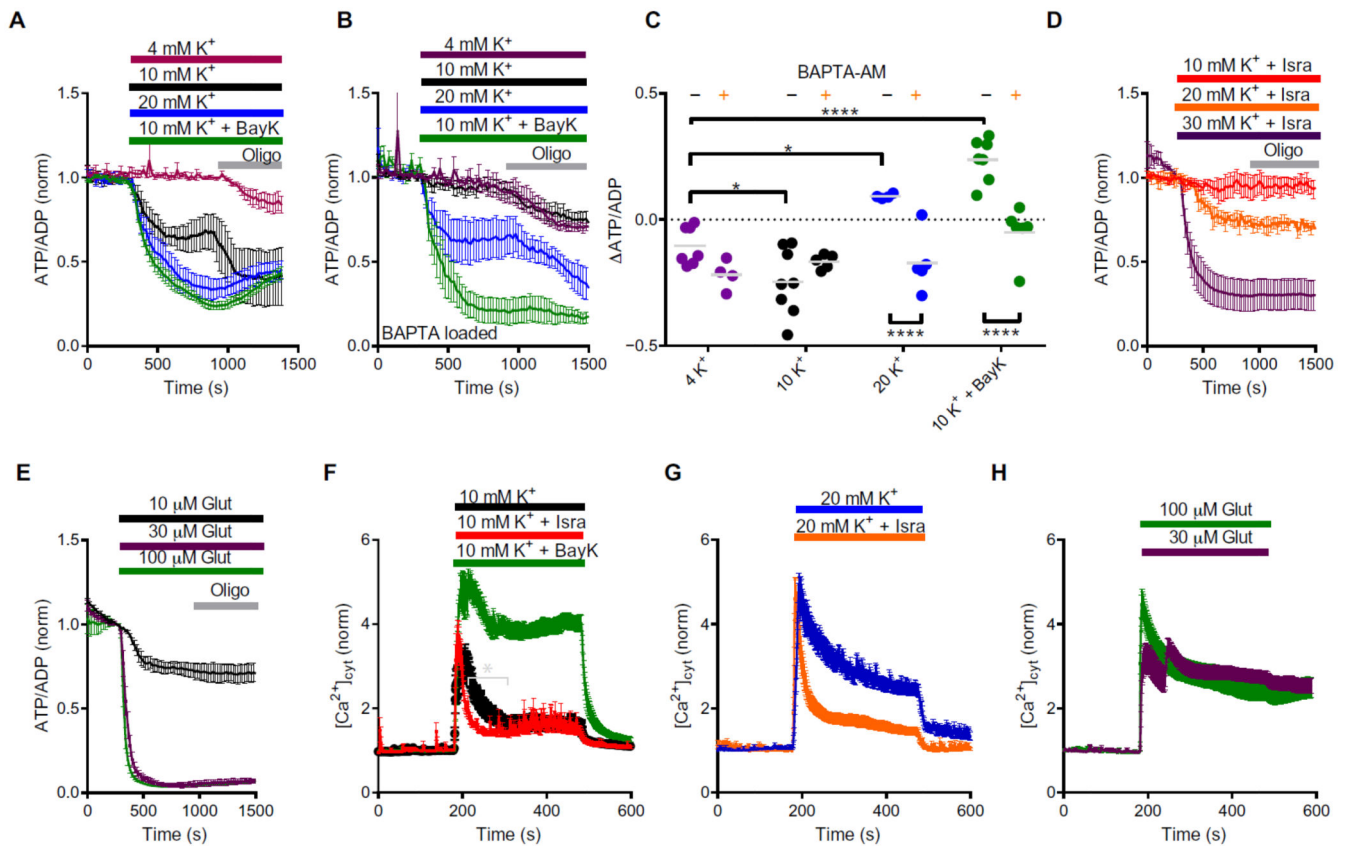


Fig. 1. Effects of neuronal stimulation on the cytosolic ATP/ADP ratio and the cytosolic free Ca^{2+} concentration.

The application of test solutions is indicated by color-coded horizontal bars. Oligomycin (Oligo) was co-applied during the experiment as indicated by the gray bar. Graphs show mean data points and standard errors of the mean (SEM). (A) Effect of changing the extracellular K^+ concentration and of the subsequent application of oligomycin on the ATP/ADP ratio. $n=3$ (4 mM K^+), $n=5$ (10 mM K^+), $n=5$ (20 mM K^+) and $n=6$ (10 mM K^+ + BayK). (B) Effect of changing the extracellular K^+ concentration and of the subsequent application of oligomycin on the ATP/ADP ratio in neurons pre-treated with BAPTA-AM ($n=4-6$). (C) Quantification and statistical evaluation of the change in ATP/ADP ratio ($\Delta ATP/ADP$) upon application of oligomycin in A and B ($n=4-8$). ****, $P < 0.0001$; ***, P 0.0001 to 0.001; **, P 0.001 to 0.01; *, P 0.01 to 0.05 (one-way ANOVA with Bonferroni's multiple comparisons test). (D) Effect of changing the extracellular K^+ concentration and of the subsequent application of oligomycin on the ATP/ADP ratio in the presence of isradipine (Isra, $n=3-5$). (E) Effect of application of glutamate at the indicated concentrations and of subsequent oligomycin application on the ATP/ADP ratio. Isradipine was present in all experiments ($n=3-5$). (F) Effect of 10 mM K^+ -stimulation with or without LTCC modulators on the cytosolic free Ca^{2+} concentration ($[Ca^{2+}]_{cyt}$). In the solution without a dihydropyridine, only the solvent DMSO was present. $n=9$ (+DMSO, 10 mM K^+ only); $n=6$ (+BayK), $n=6$ (+Isra). The asterisk indicates significant differences (P value between 0.01 and 0.05) between the data points outlined by square brackets, as revealed by t-test. (G) Effect of 20 mM K^+ -stimulation with or without isradipine (Isra) on the cytosolic free Ca^{2+}

concentration ($[Ca^{2+}]_{cyt}$); n=12 (+DMSO, 20 mM K^+ only); n=6 (+Isra). **(H)** Effect of glutamate application in the indicated concentrations in the presence of isradipine on $[Ca^{2+}]_{cyt}$. n=25 (30 μ M glutamate) and n=13 (100 μ M glutamate). For (A) to (H), n represents the number of neurons investigated in at least 3 separate culture dishes.

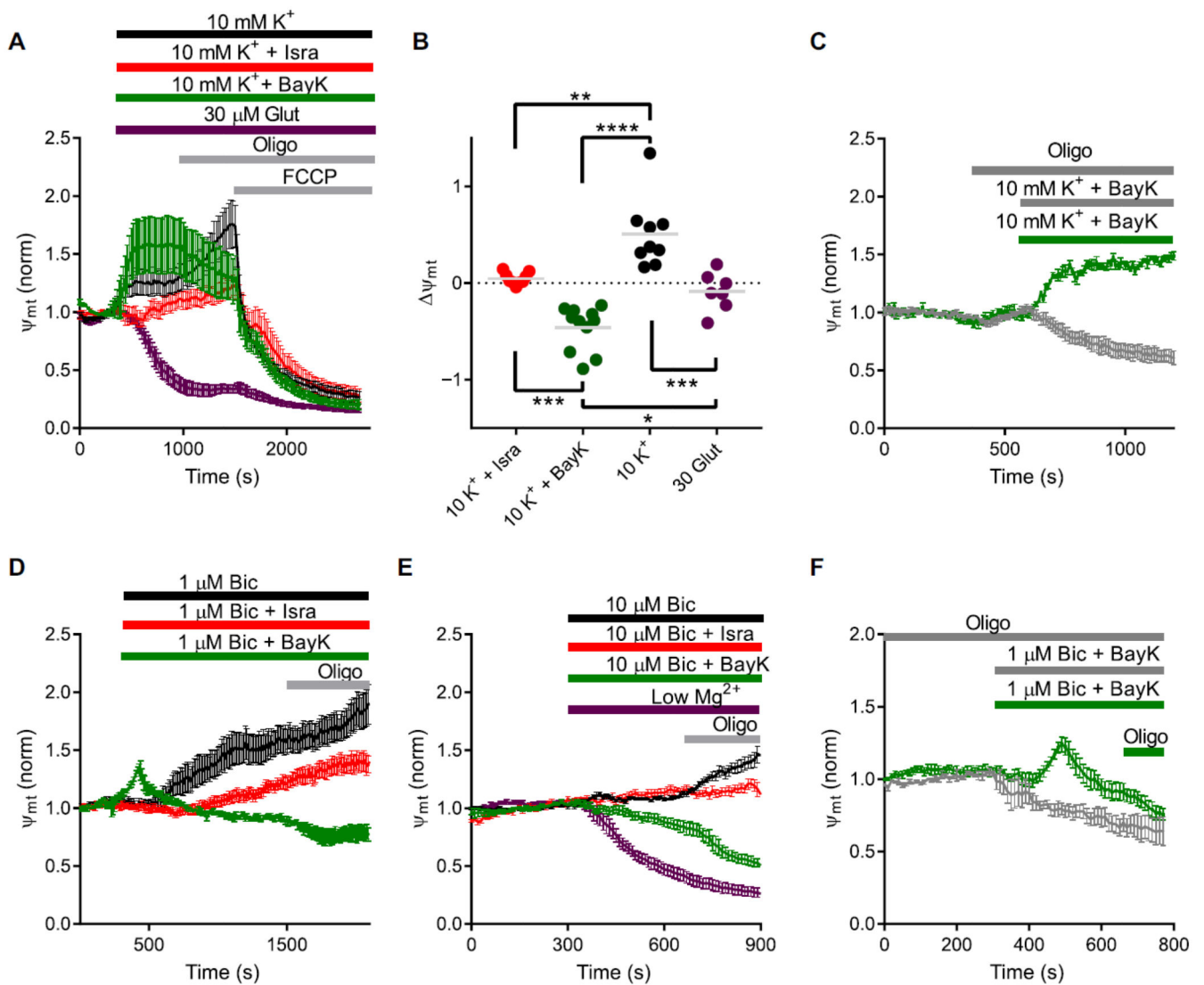


Fig. 2. Effects of neuronal stimulation on the mitochondrial membrane potential.

(A) Effect of the application of the indicated test solutions (indicated by color-coded horizontal bars) on Ψ_{mt} . Oligomycin and FCCP were applied during the experiment as indicated by the gray bars ($n=5-10$). (B) Ψ_{mt} in response to oligomycin in A were quantified and are shown with statistical evaluation in the scatter plot. ($n=7-11$). ****, $P < 0.0001$; ***, $P 0.0001$ to 0.001 ; **, $P 0.001$ to 0.01 ; *, $P 0.01$ to 0.05 (one-way ANOVA with Bonferroni's multiple comparisons test). (C) Effect of 10 mM K^+ + BayK in the absence (green trace) ($n=4$) or presence of pre-applied oligomycin (gray trace) on Ψ_{mt} ($n=5$). (D) Effect of the application of $1 \text{ }\mu\text{M Bic}$ without or with BayK or Isra and subsequent co-application of oligomycin on Ψ_{mt} ($n=3-7$). (E) Effect of the application of $10 \text{ }\mu\text{M Bic}$ without or with BayK or Isra and subsequent co-application of oligomycin on Ψ_{mt} ($n=3-7$). The effect of low Mg^{2+} solution and subsequent co-application of oligomycin is also shown in the purple trace. (F) Effect of $1 \text{ }\mu\text{M Bic}$ + BayK in the absence (green trace) or presence of pre-applied oligomycin (gray trace) ($n=4$ for each

trace). For (A) and (B), n represents the number of neurons investigated in 3 separate culture dishes. For (C) to (F), n represents the number of neurons investigated in 2 separate culture dishes.

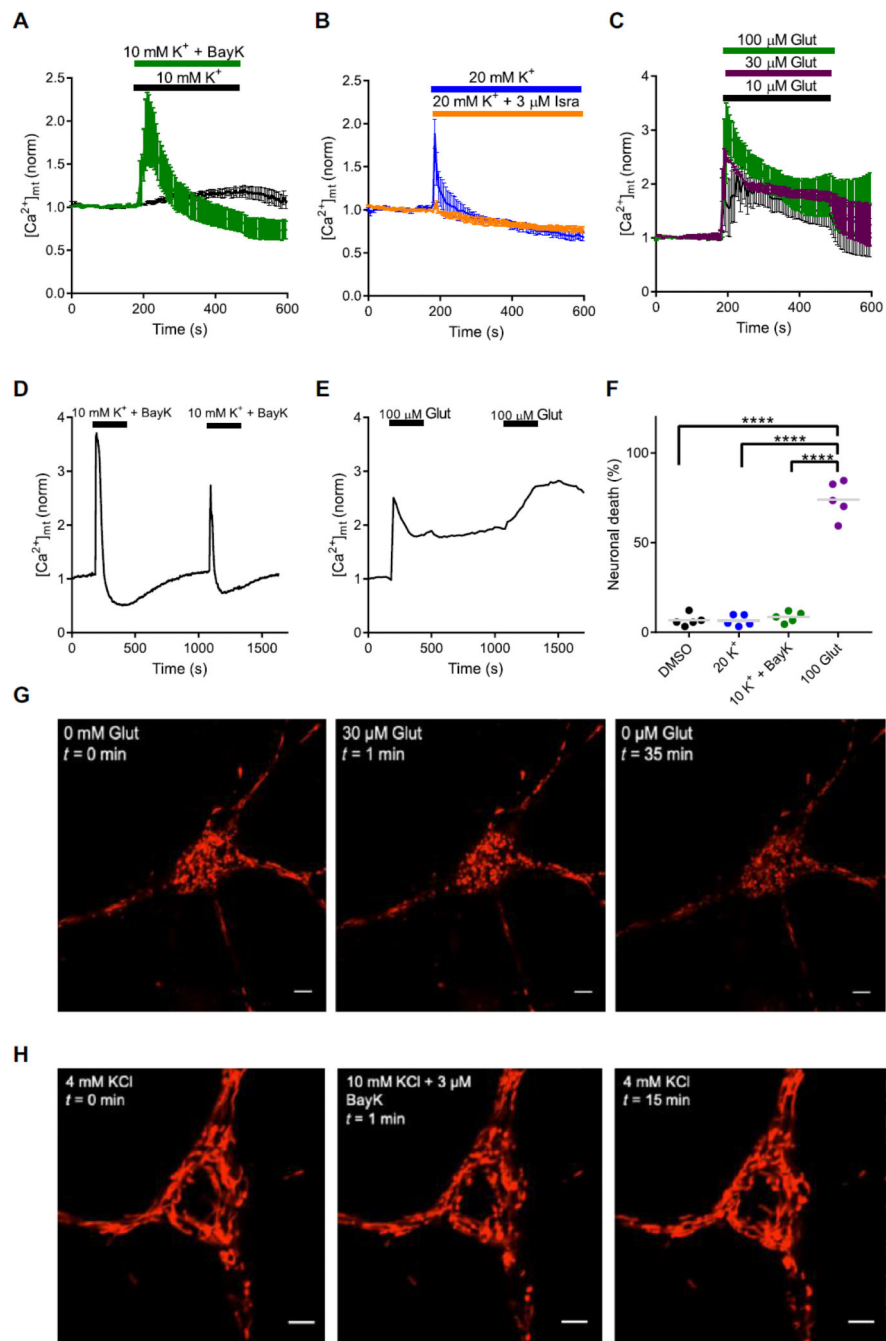


Fig. 3. Effects of neuronal stimulation on mitochondrial free Ca^{2+} concentration, neuronal death and mitochondrial morphology.

(A) Mitochondrial Ca^{2+} signals induced by 10 mM K^+ (black trace, n=6) and 10 mM K^+ + BayK (green trace, n=6). (B) Mitochondrial Ca^{2+} signals induced by 20 mM K^+ (blue trace, n=3) and 20 mM K^+ + isradipine (orange trace, n=6). (C) Mitochondrial Ca^{2+} signals induced by 10, 30 and 100 μ M glutamate (in the presence of isradipine, n=3-4). In (A) to (C), n represents the number of neurons investigated in separate culture dishes. (D) Mitochondrial Ca^{2+} transients evoked by repeated application of 10 mM K^+ + BayK in the

same neuron (representative of 3 independent experiments performed in separate culture dishes). **(E)** Elicitation of a persistent mitochondrial Ca^{2+} elevation during the course of repeated application of glutamate (representative of 5 independent experiments performed in separate culture dishes). **(F)** Effect of RMO-inducing solutions on neuronal death determined in a propidium iodide assay (n=5 separate culture dishes). ****, $P < 0.0001$ (one-way ANOVA with Bonferroni's multiple comparisons test). **(G)** Morphological changes in mitochondria fluorescently-labeled with mito-DsRed upon application of 100 μM glutamate (representative of 5 independent experiments performed in separate culture dishes). **(H)** Morphological changes of mitochondria fluorescently-labeled with mito-DsRed upon application of 10 mM K^+ + BayK (representative of 3 independent experiments performed in separate culture dishes). Scale bar in G and H, 5 μm .

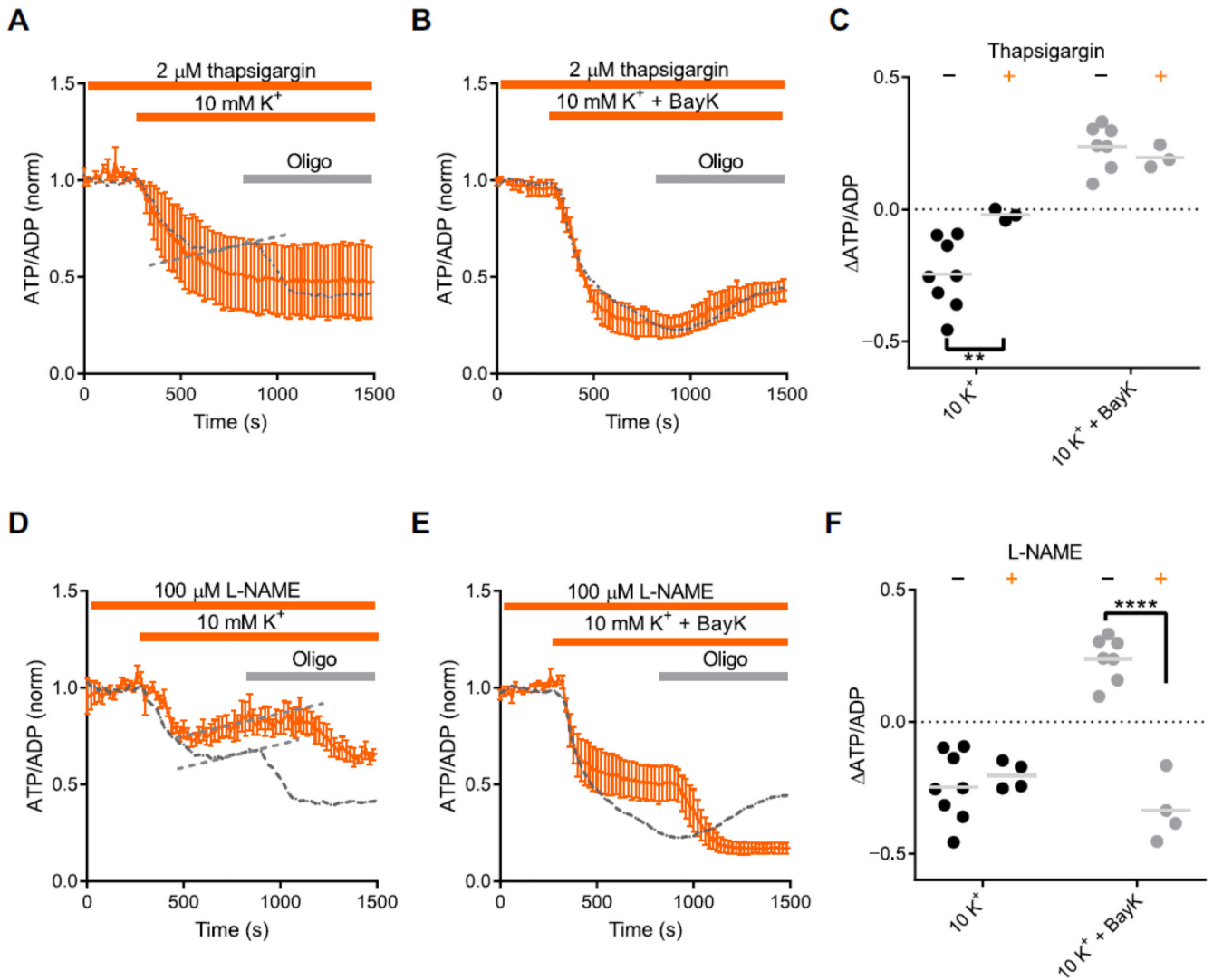


Fig. 4. Analysis of the involved intracellular signaling cascades.

(A) Effect of 10 mM K⁺ and of subsequent co-application of oligomycin on the ATP/ADP ratio in neurons pre-treated with thapsigargin. The dotted gray line retraces the corresponding data from Fig. 1A in all graphs; the dashed line highlights the trend towards a relative increase during the later phase of the response (n=3). (B) Effect of 10 mM K⁺ + BayK and of subsequent co-application of oligomycin on the ATP/ADP ratio in neurons pre-treated with thapsigargin (n=3). (C) Scatter plot showing the oligomycin responses during stimulation with 10 mM K⁺ and 10 mM K⁺ + BayK in the presence (n=3 in both cases) or absence (n=8 and n=7, respectively) of thapsigargin. **, P 0.001 to 0.01 (one-way ANOVA with Bonferroni's multiple comparisons test). (D) Effect of 10 mM K⁺ and of subsequent co-application of oligomycin on the ATP/ADP ratio in neurons pre-treated with L-NAME (n=4). (E) Effect of 10 mM K⁺ + BayK and of subsequent co-application of oligomycin on the ATP/ADP ratio in neurons pre-treated with L-NAME (n=4). (F) Scatter plot showing the changes in the ATP/ADP ratio in response to oligomycin without (-) and with (+) L-NAME (as indicated) during stimulation with 10 mM K⁺ (-: n=8; +: n=4) and 10 mM K⁺ + BayK (-:

n=7; +: n=4). ****, $P < 0.0001$ (one-way ANOVA with Bonferroni's multiple comparisons test). For (A) to (F), n represents the number of neurons investigated in separate culture dishes.

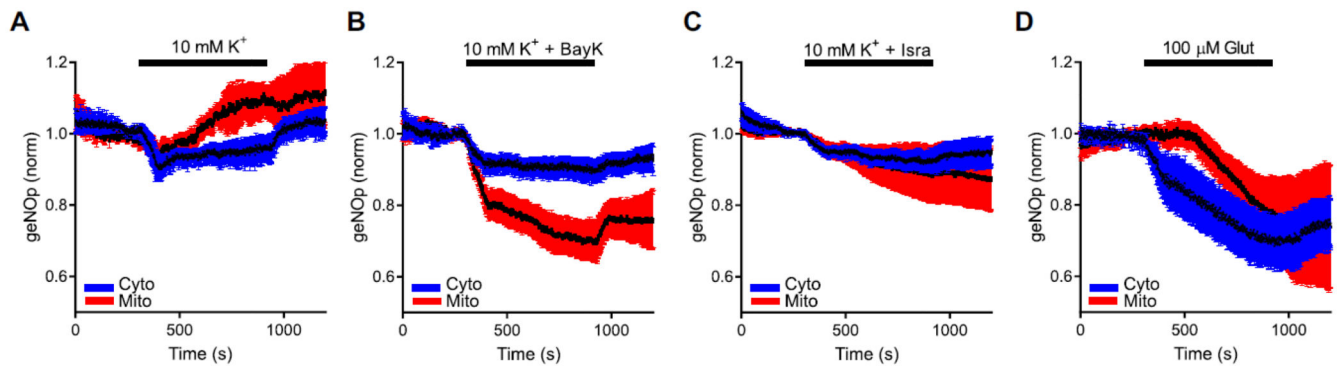


Fig. 5. Stimulation-induced changes in cytosolic and mitochondrial nitric oxide production. (A to D) Effect on the fluorescence of the geNOp probe targeted to the cytosol or the mitochondrial matrix elicited by stimulation with 10 mM K⁺ (n=3) (A), 10 mM K⁺ + BayK (n=4) (B), 10 mM K⁺ + Isra (n=6) (C), and 100 μM glutamate (n=3) (D). For (A) to (D), n represents the number of neurons investigated in separate culture dishes.

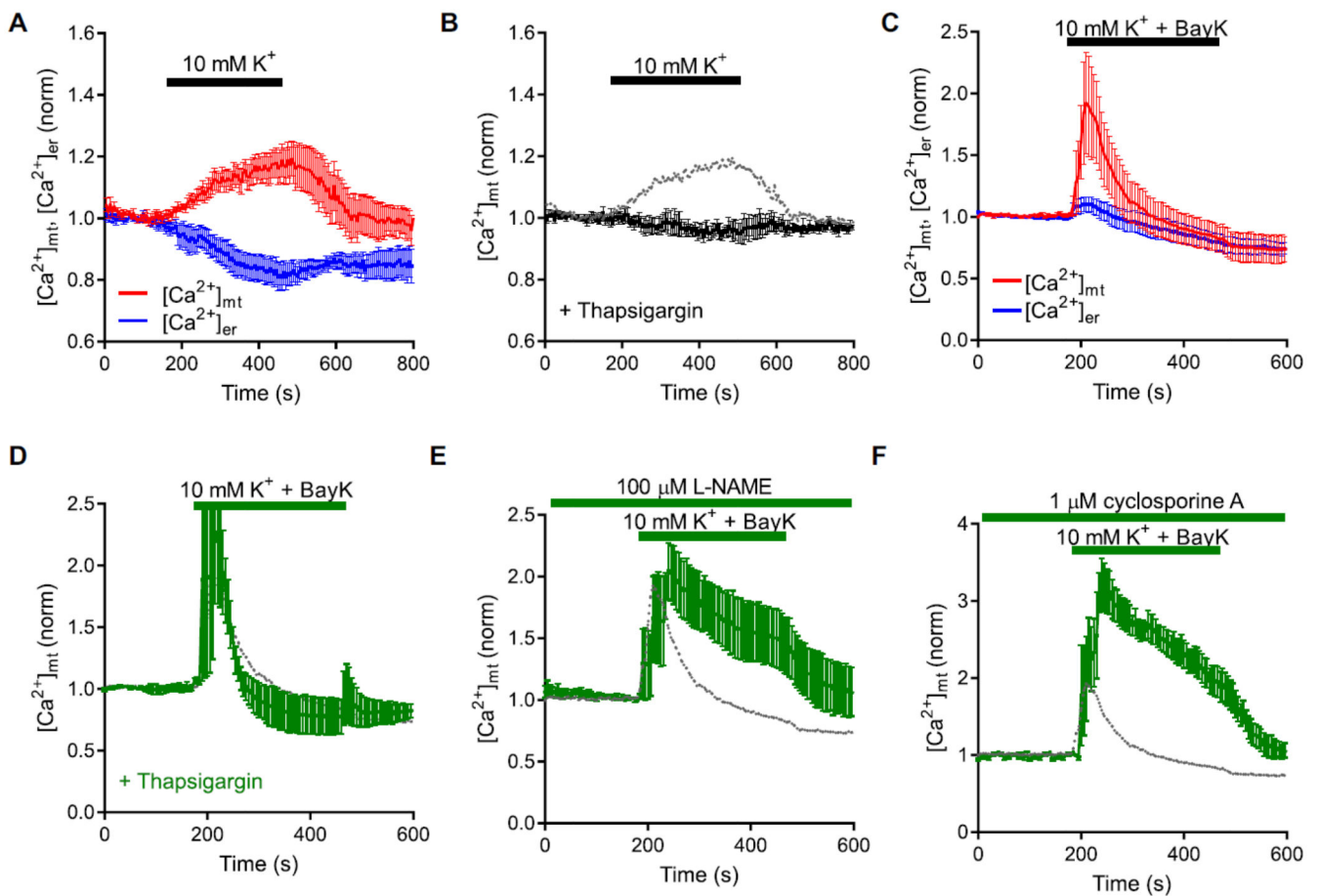


Fig. 6. Analysis of mitochondrial Ca^{2+} elevations.

(A) Changes in mitochondrial free Ca^{2+} and of free Ca^{2+} in the ER upon stimulation with 10 mM K^+ (application indicated by the black horizontal bar) (n=6). (B) Changes in mitochondrial free Ca^{2+} upon stimulation with 10 mM K^+ in neurons pre-treated with thapsigargin (n=3). The dotted gray line retraces the data in (A) from neurons not treated with thapsigargin. (C) Changes in mitochondrial free Ca^{2+} and of free Ca^{2+} in the endoplasmic reticulum (ER) upon stimulation with 10 mM K^+ + BayK (application indicated by the black horizontal bar) (n=6). (D) Changes in mitochondrial free Ca^{2+} upon stimulation with 10 mM K^+ + BayK in neurons pre-treated with thapsigargin (n=3). The dotted gray line retraces the data in (C) from neurons not treated with thapsigargin. (E) Effect of stimulation with 10 mM K^+ + BayK on the concentration of mitochondrial free Ca^{2+} in the continuous presence of L-NAME (green trace, n=3). (F) Effect of stimulation with 10 mM K^+ + BayK on the concentration of mitochondrial free Ca^{2+} in the continuous presence of cyclosporine A (green trace, n=4). The dotted gray lines in (E) and (F) retrace data from untreated neurons in (C) (red trace). In (A) to (F), n represents the number of neurons investigated in separate culture dishes.

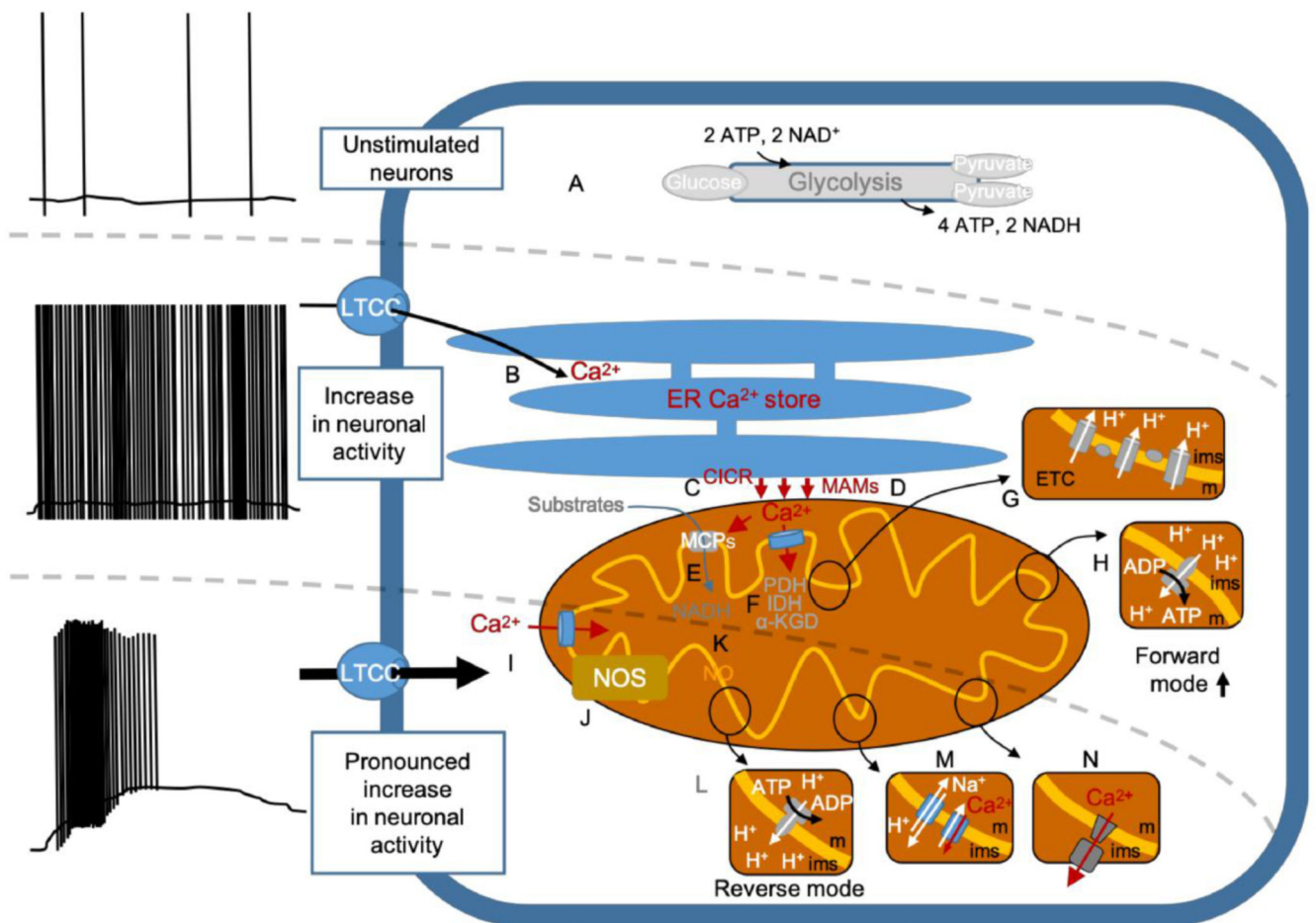


Fig. 7. LTCC-dependent regulation of the mitochondrial ATP synthase in response to various neuronal discharge activities.

(A) Glycolysis. (B) LTCC-mediated Ca²⁺ influx. (C) Ca²⁺-induced Ca²⁺ release, CICR. (D) Mitochondria-associated membranes, MAMs. (E) Mitochondrial carrier proteins, MCP. (F) Pyruvate dehydrogenase, PDH; isocitrate dehydrogenase, IDH; α -ketoglutarate dehydrogenase, α -KGD. (G) Electron transport chain, ETC. (H) ATP synthase operating in forward mode. (I) Mitochondrial Ca²⁺ rise. (J) Mitochondria-associated nitric-oxide synthase, NOS. (K) Nitric oxide, NO. (L) ATP synthase operating in reverse mode. (M) H⁺-driven Na⁺ extrusion and mitochondrial Na⁺/Ca²⁺ exchanger. (N) Mitochondrial permeability transition pore, mPTP. ATP, adenosine triphosphate; ims, intermembrane space; m, mitochondrial matrix; NAD⁺ and NADH, oxidized and reduced form of nicotinamide adenine dinucleotide.